

A Thesis

entitled

Application of Mass Spectrometry to the Characterization of Core and Ligand Shell  
Modifications of Silver Monolayer-Protected Clusters.

by

Tharuka Ubayasena

Submitted to the Graduate Faculty as partial fulfillment of the requirements for the  
The Master of Science Degree in Chemistry

---

Dr. Terry P. Bigioni, Committee Chair

---

Dr. Mark R. Mason , Committee Member

---

Dr. Dragan Isailovic, Committee Member

---

Dr. Amanda C. Bryant-Friedrich, Dean  
College of Graduate Studies

The University of Toledo

December 2020

Copyright, December 2020, Tharuka Ubayasena

This document is copyrighted material. Under copyright law, no parts of this document may be reproduced without the expressed permission of the author.

An Abstract of  
Application of Mass Spectrometry to the Characterization of Core and Ligand Shell  
Modifications of Silver Monolayer-Protected Clusters

by

Tharuka Ubayasena

Submitted to the Graduate Faculty as partial fulfillment of the requirements for the  
Master of Science Degree in Chemistry

The University of Toledo

December 2020

Monolayer protected clusters (MPCs) possess unique physicochemical properties such as well-defined molecular structures (i.e., they are a class of molecular nanoparticles), discrete electronic transitions, and strong luminescence that are not accessible to conventional nanoparticles. Such unique properties, along with ultrasmall size and biocompatibility, enable these MPCs to be successfully used in a wide range of applications, including imaging, sensing, catalysis, and as antimicrobial agents. As a result, synthesis and structural determinations of MPCs have gained great research interest in the nanoparticle community. Over the past two decades, many groups were able to synthesize metal MPCs with various nuclearities. In addition, structural identification and molecular formula determinations have become feasible with improvements in characterization techniques such as high-resolution mass spectrometry (HRMS) and single-crystal X-ray diffraction (XRD).

Despite the advancements in synthesis and structural determination, the mechanistic means of post-synthetic modifications of these MPCs, such as surface

modification and alloying, remain largely unexplored. It is crucial to understand the reactivity of MPCs in order to exploit their applicability in different fields. The key to the understanding of such reactions is the ability to characterize MPCs precisely.

There are many techniques that are commonly used to characterize MPCs, including optical absorption spectroscopy, transmission electron microscopy (TEM), nuclear magnetic resonance (NMR) spectroscopy, vibrational spectroscopy, and HRMS. HRMS is unique compared to the other techniques because, as an analytical tool, HRMS can perform three main tasks: measuring core composition, characterizing ligand shell, and determining the molecular formula (including intrinsic charge) for MPCs simultaneously. Additionally, the unique isotopic patterns and fragmentation data from mass spectrometry enables the characterization of MPCs. Various advanced mass spectrometric techniques such as high-resolution electrospray ionization mass spectrometry (HR-ESI MS) and matrix-assisted laser desorption mass spectrometry (MALDI MS) have become more utilized in the characterization of MPCs.

In the first part of the thesis, the all-silver  $M_4Ag_{44}(p-MBA)_{30}$  MPC was used as a model platform to study post-synthetic galvanic substitution reactions, where M is a mono cationic counterion, and p-MBA is para-mercaptobenzoic acid. Gold was chosen as a hetero metal for the substitution because gold and silver are isoelectronic and have the same atomic radius, and a variety of hetero ligands (SR = thiolate) were used in conjunction with the gold. Metal core modifications were carried out by galvanic exchange reaction with a Au(SR) polymer, substituting gold for silver to form  $M_4Au_xAg_{44-x}(p-MBA)_{30}$  and  $M_4Au_xAg_{44-x}(p-MBA)_{30-y}(SR)_y$  clusters. The range of product composition was determined, and the patterns of product distributions were

evaluated. Moreover, chemical properties such as stability and reactivity were studied as a function of product composition.

The electronic and steric effects of ligands in ligand exchange reactions were investigated using the same model system,  $M_4Ag_{44}(p-MBA)_{30}$ . Several parameters, including the introduction of electronically distinct functional groups and the introduction of bulky groups, were varied to find the characteristics of thiolate-for-thiolate exchange, to synthesize  $M_4Ag_{44}(SR)_{30}$ . It has been found that most ligands preserve the precise structure of the parent particle while replacing native ligands with incoming ligands comprising a variety of functional groups.

## Acknowledgements

I would like to express my deepest appreciation and gratitude to my advisor, Prof. Terry Bigioni, Department of Chemistry and Biochemistry, University of Toledo, for his guidance, continuous encouragement, and support. It was a great privilege and honor to work with him. I would also like to express my gratitude to the committee members Prof. Mark Mason and Prof. Dragan Isailovic, for the valuable advice, suggestions, and discussions. I am sincerely thankful to all my present and past lab members Dr. Zaker, Dr. Bhattarai, Abdullah, Thisari, and Ramesh, for their support. I would like to give my special thanks to Dr. Zaker for his invaluable guidance in my research.

I would like to thank the Department of Chemistry and Biochemistry and the University of Toledo for giving me the opportunity to pursue my higher education. I would also like to thank the staff from the Instrumentation Center and Chemical Stockroom for their help throughout this time. Last but certainly not least, I am extremely thankful to my family for their love and support.

# Table of Contents

Abstract.....	iii
Acknowledgements.....	vi
Table of Contents.....	vii
List of Figures.....	x
List of Abbreviations.....	xii
List of Symbols.....	xiii
1 Introduction	
1.1 Evolution of nanotechnology.....	1
1.2 Nanoparticles.....	2
1.3 Monolayer-protected clusters (MPCs).....	3
1.4 Stability of metal MPCs.....	5
1.5 Characterization techniques for metal MPCs.....	7
1.6 Mass spectrometric analyses of metal MPCs.....	8
1.7 Objectives of the research.....	9
2 Metal exchange of monolayer protected clusters	
2.1 Introduction.....	11
2.2 Experimental.....	13

	2.2.1 Chemicals.....	13
	2.2.2 Synthesis of $M_4Au_xAg_{44-x}(p-MBA)_{30-y}(SC_6H_4OH)_y$ by Galvanic Exchange.....	14
	2.2.3 Synthesis of gold thiolate.....	14
	2.2.4 Optical measurements.....	15
	2.2.5 Electrospray ionization mass spectrometry (ESI-MS).....	16
	2.3 Results and Discussion .....	17
	2.4 Conclusions.....	24
3	Ligand Exchange reactions of MPCs	
	3.1 Introduction.....	25
	3.2 Experimental .....	28
	3.2.1 Chemicals.....	28
	3.2.2 Electrospray ionization mass spectrometry .....	29
	3.3 Results and Discussion .....	29
	3.3.1 Preferential exchange sites.....	29
	3.3.2 Nature of the substitution.....	32
	3.4 Conclusion .....	35
4	Conclusions .....	36
	References.....	43

## List of Figures

1 – 1	The cluster abundance spectrum of gas phase sodium clusters .....	11
1 – 1	Optical absorption spectra of $M_4Au_xAg_{44-x}(p-MBA)_{30-y}(SC_6H_4OH)_y$ species synthesized .....	24
2 – 2	ESI-MS spectra showing the distribution of $M_4Au_xAg_{44-x}(pMBA)_{30-y}(SC_6H_4OH)_y$ species synthesized by galvanic exchange .....	25
2 – 3	Rescaled ESI-MS spectra showing the distribution of $M_4Au_{x+1}Ag_{43-x}(SC_6H_4OH)_y$ species .....	26
2 – 4	Gaussian fits to metal atom substituted peak distributions .....	28
2 – 5	Gaussian fits to metal atom exchange with one ligand .....	29
2 – 6	Gaussian fits to metal atom exchange with two ligands .....	29
3 – 1	Structure of a $Na_4Ag_{44}(p-MBA)_{30}$ mNP .....	33
3 – 2	Negative-ion ESI mass spectra of the products prepared by reaction of $Na_4Au_{44}(p-MBA)_{30}$ with SHPhOH in DMF at different input ratios .....	36
3 – 3	Negative-ion ESI mass spectra of the products prepared by reaction of $Na_4Au_{44}(p-MBA)_{30}$ with (4-FTP) in DCM at different input ratios .....	37
3 – 4	Negative-ion ESI mass spectra of the products prepared by reaction of $Na_4Au_{44}(p-MBA)_{30}$ with 4-FTP, 4-CTP and, 4-BTP in DCM at 1:1 input ratio .....	39
3 – 5	Rescaled ESI mass spectra of the products prepared by reaction of $Na_4Au_{44}(p-MBA)_{30}$ with 4-FTP, 4-CTP and, 4-BTP in DCM at 1:1 input ratio .....	40

## List of Abbreviations

AFM.....	Atomic Force Microscopy
BTP.....	Bromothiophenol
CTP.....	Chlorothiophenol
DFT.....	Density Functional Theory
DMF.....	Dimethylformamide
DMSO.....	Dimethyl Sulfoxide
ESI.....	Electrospray Ionization
HOMO.....	Highest Occupied Molecular Orbital
HPLC.....	High performance liquid chromatography
HSC <sub>6</sub> H <sub>4</sub> OH.....	Mercaptophenol
IR.....	Infrared Spectroscopy
LUMO.....	Lowest Unoccupied Molecular Orbital
LDI.....	Laser Desorption Ionization
MALDI.....	Matrix-Assisted Laser Desorption Ionization
MNP.....	Molecular Nanoparticle
MPC.....	Monolayer-Protected Clusters
MS.....	Mass Spectroscopy
NMR.....	Nuclear Magnetic Resonance Spectroscopy
p-MBA.....	para-mercaptobenzoic acid
SEM.....	Scanning Electron Microscopy
SR.....	Thiolate
STM.....	Scanning Tunneling Microscopy
TEM.....	Transmission Electron Microscopy
UV-Vis.....	Ultraviolet-visible Spectroscopy
XRD.....	X-ray Diffraction

## List of Symbols

$v$	.....	Number of valence electrons of the metal
$e^-$	.....	Electron
$L$	.....	Number of ligands
$M$	.....	Number of metal atoms
$n^*$	.....	Number of electrons
$y$	.....	Number of substituted ligands
$x$	.....	Number of delocalized electrons in a nanocluster
$Z$	.....	Overall nanocluster charge

# Chapter 1

## Introduction

### 1.1 Evolution of nanotechnology

Although nanotechnology is a fairly new area of science, the main concepts have been developing over the last fifty years. But most interestingly, people have been employing nanotechnology for over more than a thousand years for various purposes. For example, the evidence of usage of nanomaterials dates back to the fourth century, where Romans used nano-sized metals to decorate glasses and cups. One of the most famous examples is the Lycurgus cup, in which the glass was embedded with nanoparticles of gold and silver that changes color depending on the location of the light source. Besides the Romans, medieval stained-glass artisans also explored the effect of the addition of small metal particles in glass to create colored glass windows. They trapped gold and silver nanoparticles in the 'glass matrix' to generate the ruby red and deep yellow colors in the windows. The use of nano-sized metals had been extended even to areas in medieval medicine<sup>1</sup> and ceramics.<sup>2</sup>

However, scientific interest in nanoparticles did not begin until the synthesis of colloidal suspensions of gold by Michael Faraday in the mid-1850s. He was able to

synthesize the "ruby-colored" solution by reducing gold chloride.<sup>3</sup> Although his work was groundbreaking, it was not well understood at that time due to the limited availability of characterization technology and lack of knowledge in areas such as quantum science. But since the invention of the electron microscope and the emergence of quantum mechanics in the early 1900s, the development of nanotechnology has significantly accelerated.

One of the revolutionary points in nanotechnology's history came in a lecture by the great physicist Richard Feynman in 1959, entitled 'There is plenty of room at the bottom' (Feynman, 1959).<sup>4</sup> During his talk, he highlighted the possibility of working at a micro-and nanoscale and discussed the controlling of atoms and molecules and their subsequent manipulation on a small scale.

His words motivated researchers to build up new instruments and technologies with atomic precision. With the invention of the scanning tunneling microscope (STM), atomic force microscopy (AFM), scanning electron microscopy (SEM), transmission electron microscopy (TEM), and other modern instruments, it is possible to study nanoparticles at the atomic level. These recent innovations have expanded the ability to control and engineer nanomaterials, making this area a hot topic in material science and engineering.

## **1.2 Nanoparticles**

A nanoparticle can be defined as a particle with at least one dimension in the range of a 1-100 nm. Thus, a nanoparticle could be one dimensional such as nanowires, or it could be two dimensional such as a thin surface or a coating whose thickness is on a

nanometer scale. The nanoparticles, colloids, and quantum dots (small particles of semiconductor materials) fall in the category of three-dimensional nanomaterials.

Nanoparticles usually have different sizes. The properties and applications of nanoparticles depend on their size. For conventional colloidal nanoparticles, the optical and electronic properties change monotonically (i.e., their properties scale with their size). But nanoparticles with smaller sizes (<3 nm) can show discrete optical and electronic properties that do not scale with their size and behave more like molecules.

### **1.3 Monolayer-protected clusters (MPCs)**

Metal monolayer-protected clusters (MPCs) are a relatively new form of nanomaterials composed of a precise number of metal atoms and organic ligands.<sup>5-6</sup> The atomically precise MPCs differ from other unprotected nanoparticles mainly due to their ultra-small core size (<3 nm).<sup>7</sup> A monolayer protected cluster is composed of two defining parts-metal core and protecting ligands, which dominate the character of these nanoparticles. These MPCs generally show quantum properties, such as tunable band gaps with HOMO-LUMO transitions, quantized charging, strong luminescence, and discrete optical absorbance bands.<sup>7-10</sup> Therefore, considering their well-defined molecular structure and property together, MPCs could also be referred to as "molecular nanoparticles." Extensive research is currently being carried out to assess possible applications of MPCs in which their size-specific physical and chemical properties would be advantageous. Potential applications are expected to be found in various fields, including sensing, imaging, antimicrobials, and catalysis.

Moreover, the atomic precision in synthesis and ease of tracking the size and structure evolution suggest these metal NCs as an ideal model platform for pursuing total synthesis chemistry of monolayer protected Nobel metal clusters.

Like any other molecular species, monolayer-protected clusters (MPCs) or molecular nanoparticles (MNPs) can be identified by their molecular formula. MPCs have particle sizes less than 3 nm. MPCs are atomically precise. MPCs also have a specific molecular structure.<sup>11</sup> Generally, MPCs have two distinct parts in their structure. The inorganic metal forms the core of the MPCs. Organic ligands form a passivation shell, typically forming capping motifs with the metal to protect the inner metallic core. MPCs have the potential for several important applications such as antimicrobials, catalysis, and bio-imaging due to their unique optical and electronic properties.<sup>12-15</sup>

The synthesis of metal MPCs was first reported in the early 1990s, ultimately derived from colloidal particles. In 1994, the Whyman group from the University of Liverpool synthesized gold MPCs using a two-phase method.<sup>16</sup> The Whetten group from the Georgia Institute of Technology reported an improved synthesis of gold MPCs along with their mass spectrometric analysis in 1996.<sup>17</sup> The Murray group from the University of North Carolina at Chapel Hill also reported similar results around that time.<sup>18-20</sup>

In 2004, the Tsukuda group demonstrated the synthesis of a magic-number series of gold-glutathione (Au:SG) MPCs in a one-pot reaction, and they were able to correctly assign molecular formulae to some of the Au:SG MPCs.<sup>21-22</sup> In 2007, the Kornberg group published the first-ever crystal structure of a metal MPC ( $[\text{Au}_{102}(\text{p-MBA})_{44}]$ , where *p*-MBA = *para*-mercaptobenzoic acid) in *Science*.<sup>23</sup> In 2009, the Stellacci group reported the so-called intensely and broadly absorbing nanoparticles (IBANs), which were silver

MPCs protected by aryl-thiol ligands.<sup>24</sup> IBANs showed molecular signatures in their optical spectra that were completely different from plasmonic nanoparticles and were later identified as  $[\text{Ag}_{44}(\text{SR})_{30}]^{4-}$  MPCs.<sup>25</sup> In 2010, the Bigioni group reported the synthesis of a magic-number series of silver-glutathione (Ag:SG) (where SG is deprotonated glutathione) MPCs in a one-pot reaction.<sup>26</sup> They later reported the crystal structure of  $[\text{Ag}_{44}(\text{p-MBA})_{30}]^{4-}$  MPCs in 2013 in *Nature*.<sup>11</sup> The crystal structures allowed a deeper understanding of these MPCs.

## 1.4 Stability of metal MPCs

The notion of an electronic origin of cluster stability was developed when Knight *et al.* used gas-phase mass spectrometry of sodium metal clusters and observed some

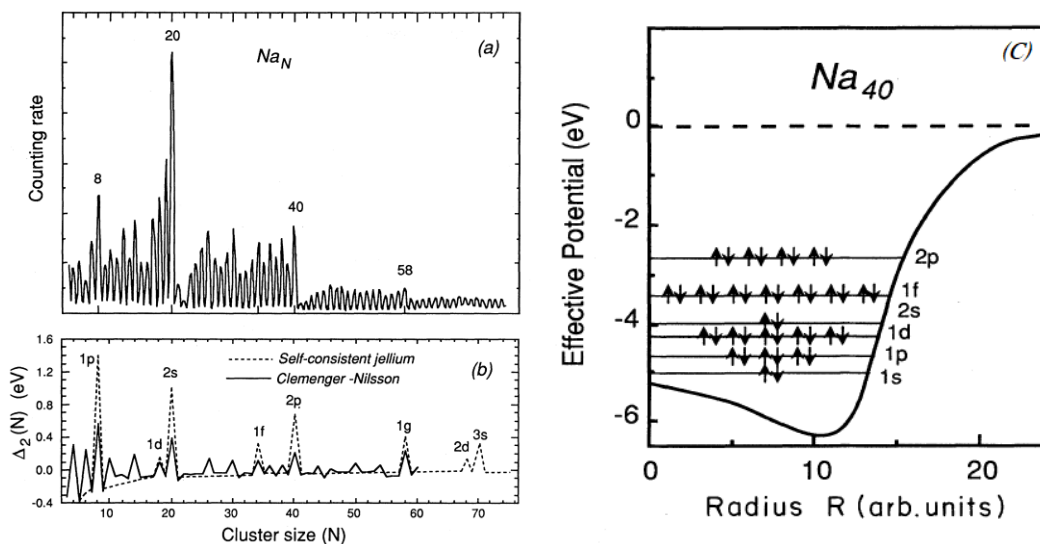


**Figure 1-1.** The cluster abundance spectrum of gas phase sodium clusters (a) Experimental (b) Theoretical and (c) The calculated effective potential for  $\text{Na}_{40}$  gas phase cluster with filled energy levels. Reprinted with permission from reference 28. Copyright 1993 American Physical Society.

clusters were more abundant than others. The sodium metal clusters of  $N = 8, 20, 40, 58,$

and 92, where N is the number of Na atoms, showed higher abundances when compared to other nanoclusters. They believed that the stability of sodium nanoclusters with "magic numbers" corresponding to  $N = 8, 20, 40, 58,$  and 92 was due to a closed electron shell (Figure 1-1a). These results compared favorably with theoretical models (Figure 1-1b).<sup>27</sup>

The stability of these particles has been explained by the "superatom electronic theory," which is based on a Jellium model. The Jellium model is a quantum mechanical model for delocalized electrons in solids where the positive charges are assumed to be uniformly distributed in space. According to the jellium model, a cluster is treated as an object consisting of two parts: a system of valence electrons and an ionic core. From the theoretical point of view, the nanocluster's electronic and optical properties were successfully described by means of the Jellium model<sup>28-30</sup>. And theoretically calculated electronic shell structure for a  $\text{Na}_{40}$  gas-phase cluster is shown in Figure 1-1c.

Unlike bulk materials, the energy levels in MPCs are close but do not overlap due to the quantum confinement. The superatomic orbital theory treats the metal core as a large spherical "superatom" and uses valence electrons to fill the superatomic orbitals, which are analogous to regular atomic orbitals.<sup>31</sup> One important difference is the set of angular momentum quantum numbers. The appropriate building up principle of filling delocalized electrons in "superatomic orbitals" of metal clusters is,  $1S^2 | 1P^6 | 1D^{10} | 2S^2 | 1F^{14} | 2P^6 | 1G^{18} | \dots$ , where, S–P–D–F–G–H– denote the superatomic orbitals with corresponding angular-momentum quantum numbers, with vertical lines representing closed shells.<sup>31</sup>

In the solution phase, clusters are protected by ligands such as thiolates through bonding with surface metal atoms. Depending on the nature of ligands, the electron count

may change. Therefore, the formula for calculating the number of free delocalized electrons is given by,

$$n = M v - L - z$$

where  $n$  is the electron count for the MPC,  $M$  is the number of metal atoms,  $v$  is the number of valence electrons of the metal,  $L$  is the number of ligands, and  $Z$  is the overall cluster charge.<sup>29</sup> For example,  $[\text{Ag}_{44}(\text{p-MBA})_{30}]^{4-}$  has 18 electrons, which is calculated as  $44 \times 1 - 30 - (-4)$ , where  $n = 44$ ,  $v = 1$ ,  $M = 30$ , and  $z = -4$ . This corresponds to the complete filling of the  $1S^2 | 1P^6 | 1D^{10} |$  based on this 18-electron count.<sup>11</sup>  $\text{Au}_{25}(\text{SR})_{18}^-$  with 8 free electrons,<sup>32</sup>  $\text{Au}_{68}(\text{SR})_{34}$  with 34 free electrons<sup>33</sup> and  $\text{Au}_{102}(\text{SR})_{44}$  with 58 free electrons.<sup>34</sup> Like any other molecule satisfies the octet rule, these ligand-protected clusters satisfy the super-atom model electronic structure.

## 1.5 Characterization techniques for metal MPCs

There are many techniques that are commonly used to characterize MPCs. For the characterization of core size, ultraviolet-visible (UV-Vis)<sup>22</sup> spectroscopy and transmission electron (TEM) microscopy can be used. UV-Vis measures the presence or absence of surface plasmon bands or characteristic absorbance spectra of MPCs, while TEM compares and contrasts core and ligand shell according to electron density.<sup>35</sup> Techniques such as nuclear magnetic resonance (NMR) or infrared spectroscopy (IR)<sup>36</sup> are used to characterize the ligand shell.<sup>35</sup> Sometimes combined techniques, such as thermal gravimetric analysis coupled with TEM, can be used to determine the approximate molecular formula of MPCs.<sup>35</sup> Mass spectrometric techniques (electrospray

ionization (ESI) and matrix-assisted laser desorption ionization (MALDI)) are widely used to assign molecular formulae of metal MPCs.<sup>37-39</sup>

## 1.6 Mass spectrometric analyses of metal MPCs

Mass spectrometry (MS) is unique compared to other techniques. As an analytical tool, MS can perform all three tasks – measuring core size, characterizing ligand shells, and determining molecular formula simultaneously. Researchers have used mass spectrometry to characterize clusters. It can give information mainly about the core size as well as the ligand shell composition. Various advanced mass spectrometric techniques such as high-resolution (HR) ESI-MS, MALDI-MS, etc., have been used to study the MPCs and thereby understand their chemistry.<sup>40</sup>

The first use of mass spectrometry in the area of gas-phase molecular clusters was reported in 1985 to identifying and understanding C<sub>60</sub> and C<sub>70</sub> clusters of the fullerene family.<sup>41</sup> Several analyses of metals such as alkali, alkaline earth, and transition metals have been studied in the gas phase.<sup>27, 42-43</sup> In most cases, magic numbers of  $n = 2, 8, 20,$  and 92 atoms have been observed as discontinuous variation in intensities. Later, mass spectrometric analysis has extended to analyze noble metal cluster systems synthesized in solution. Both Whetten and Murray groups initiated mass spectrometric characterization of such metal clusters.<sup>32, 44-46</sup> A variety of clusters having different core masses and various ligand shells have been identified at that time. In most of the cases, clusters were alkane thiol protected.<sup>47</sup> In contrast, some gold clusters were protected with glutathione,<sup>48</sup> and functionalized alkenethiols.<sup>19, 49</sup> Both TEM analysis and LDI mass spectral analysis data were used to assign molecular masses for few clusters reported around the 1990s.<sup>40,</sup>

<sup>48, 50</sup> However, some of these tentatively assigned mass numbers were reassigned later with more sensitive and high-resolution electrospray analysis.<sup>22</sup>

In the 1990s, MPC analyses only reported weights of the metal core in kDa units but not exact molecular formulas because the ionization techniques which were used at that time, such as LDI, often result in fragmentation of clusters making formula determination difficult.<sup>17</sup> Soft ionization techniques such as MALDI and ESI became more widely employed as they keep ligand-protected clusters intact during ionization. Comparatively, ESI provides gentler ionization but works best in narrow  $m/z$  range, while MALDI is more destructive but provides a higher  $m/z$  range.

## **1.7 Objectives of the research**

Metal MPCs have the potential to be used in various applications (optoelectronics, antimicrobial, bio-imaging, catalysis)<sup>51</sup> due to their well-defined molecular structure and unique physicochemical properties, such as discrete electronic transitions, and strong luminescence. Prior to applying the metal MPCs, it is necessary to precisely understand the physicochemical properties of metal MPCs. Many researchers reported synthesizing metal MPCs with various chemical compositions. Structural identification, electronic properties, and a molecular formula of those metal MPCs were studied with various analytical techniques such as UV-Vis spectroscopy, NMR, high-resolution ESI-MS, MALDI-MS, TEM, and XRD.

Despite the advancements in the synthesis and structural determination, the mechanistic means of post-synthetic modifications of these MPCs, such as surface modification and alloying, remain largely unexplored. It is crucial to understand the

reactivity of metal MPCs in order to exploit their applicability in different fields. The key to the understanding of such reactions is the ability to characterize MPCs precisely.

In the first part of the thesis, the all-silver  $M_4Ag_{44}(p-MBA)_{30}$  MPC was used as a model platform, where M is a monocationic counterion, and p-MBA serves as a protecting ligand. Metal core modifications were carried out by substituting gold for silver to form  $M_4Au_xAg_{44-x}(p-MBA)_{30}$  and  $M_4Au_xAg_{44-x}(p-MBA)_{30-y}(SR)_y$  (SR = thiolate) clusters. Gold was chosen as a hetero metal for the substitution because gold and silver are isoelectronic and have the same atomic radius. But, differences in the chemical and optical properties of the two metals provide useful contrast for the comparison. The galvanic exchange was used for the preparation of the bimetallic product. The range of product composition was determined, and the patterns of product distributions were evaluated. Moreover, chemical properties such as stability and reactivity were studied as a function of product composition.

The electronic and steric effects of ligands in ligand exchange was also investigated using the same model system,  $M_4Ag_{44}(p-MBA)_{30}$ . Several parameters, including the introduction of electronically distinct functional groups (mercaptophenol, chlorothiophenol, bromothiophenol, fluoro thiophenol) and the introduction of a bulky group (tert-butylbenzethiol), were varied to find the characteristics required for thiolate exchange to the synthesis of  $M_4Ag_{44}(SR)_{30}$ .

## Chapter 2

### Metal exchange of monolayer protected clusters

#### 2.1 Introduction

The functionalization and modification of MPC clusters in response to various applications would make them more effective as nanomaterials. Previous studies have shown that both chemical and physical properties of MPCs can be modified either by heteroatom substitution<sup>52-55</sup> or ligand substitution.<sup>56-60</sup>

The bimetallic MPCs can be synthesized by co-reduction, i.e. simultaneous reduction of two different metal precursors, or by a galvanic exchange reaction between monometallic MPCs and metal ions of a heterometal.<sup>61-62</sup> Galvanic exchange is a simple oxidation-reduction reaction that occurs when the oxidized form of metal (M1) reacts with the reduced form of metal (M2). The reaction is spontaneous when the oxidized form (M1) has a more positive standard reduction potential than that of the reduced form (M2). The atoms of M1 spontaneously replace atoms of M2 since M1 is more energetically favorable in the reduced form. Galvanic exchange in MPCs is expected to involve the same number of electrons in the oxidation and reduction reactions.

So far, three types of metal exchange reactions have been reported: (i) metal exchange with metal salts,<sup>63-64</sup> (ii) metal exchange with complexes,<sup>65-69</sup> and (iii) metal exchange between nanoclusters.<sup>70-73</sup> Thiols are the most common ligands used in these types of reactions, including metal-thiolate complexes and thiol-passivated metal MPCs.

The Murray group reported the metal exchange of MPCs using metal salts for the first time. Their attempt to exchange Au with Ag using dodecanethiolate-protected Ag clusters and H<sub>2</sub>AuCl<sub>4</sub> in THF resulted in the decomposition of Ag MPCs within ten minutes. The Au for Ag exchange reaction was successful when Au-thiolate complexes were used instead of Au salts, however<sup>69</sup>. Typically, the metal exchange reactions with metal salts are not efficient in producing alloy nanoclusters. Most of the time, these reactions only lead to few or no metal atoms exchanged, but they tend to accelerate parent nanocluster degradation. On the other hand, metal-ligand complexes and inter-cluster reactions produce alloy nanoclusters efficiently.

During these reactions, metal atoms are exchanged between metal complexes and metal clusters, thereby forming alloy clusters. Very little has been discovered in terms of the molecular-level mechanism of these reactions. However, experimental results imply that the metal exchange reaction involved in clusters below 3 nm size regime does not necessarily follow the galvanic sequence of metal activity<sup>74-75</sup>. Unlike inter-cluster metal exchange reactions, metal complex cluster reactions keep the number of constituent atoms constant during the exchange. Therefore, these reactions do not change the original geometry of a cluster while altering its composition. Compared to co-reduction (simultaneous reduction of two types of metals)<sup>76-77</sup>, this method allows a higher number of atoms with a wide range redox potentials to be exchanged more easily but in a more

controlled manner. Over the past decade, various alloy clusters such as  $\text{Au}_{25-x}\text{Ag}_x(\text{SR})_{18}$  ( $x = 1-8$ ),<sup>64, 78</sup>  $\text{Au}_{25-x}\text{Cu}_x(\text{SR})_{18}$  ( $x = 1-9$ ),<sup>78</sup>  $\text{Au}_{24}\text{Cd}(\text{SR})_{18}$ ,<sup>78-79</sup>  $\text{Au}_{24}\text{Hg}(\text{SR})_{18}$ ,<sup>78, 80</sup>  $\text{Au}_{24-x}\text{Ag}_x\text{Cd}(\text{SR})_{18}$  ( $x = 2-6$ ),<sup>81</sup>  $\text{Au}_{24-x}\text{Ag}_x\text{Hg}(\text{SR})_{18}$  ( $x = 1-8$ ),<sup>79, 81</sup>  $\text{Ag}_{25-x}\text{Au}_x(\text{SR})_{18}$  ( $x = 1, 2$ ),<sup>82-83</sup>  $\text{Ag}_{24-x}\text{Au}_x\text{Pt}(\text{SR})_{18}$  ( $x = 1, 2, 4-9$ ),<sup>68, 83</sup> and  $\text{Au}_{38-x}\text{Ag}_x(\text{SR})_{24}$  ( $x = 1-11$ )<sup>71, 84</sup> have been reported by different groups using this type of exchange reaction.

Comparatively, alloy reactions involving metal-ligand complexes produce alloy nanoclusters more efficiently than inter-cluster reactions or metal salts. A significant amount of work has already been done to establish better synthetic routes to produce alloy nanoclusters using this class of reactions. However, such synthetic pathways remain poorly understood, and mechanistic details of the reactions to explain their efficiency are still unknown.

The role of the ligand in modulating the reactivity of metal cores is well studied. In fact, in the area of colloidal nanoparticles, the ligand role in the shape-controlled growth of nanoparticles is significant.<sup>85-86</sup> How ligands affect surface reactivity of MPCs is becoming an interesting topic of investigation. Some previous metal exchange studies using ligand metal complexes led us to hypothesize that the ligand has a significant effect on metal exchange reaction.

So herein, we ask a few fundamental questions (i) Do ligands influence metal exchange and how? (ii) Do ligands exchange along with hetero metal atoms? (iii) Is there any correlation between the number of metal atoms and ligands that exchange? (iv) How does the electronic or steric nature of ligands affect the exchange process?

## 2.2 Experimental

### 2.2.1 Chemicals

The following reagents were purchased from Fisher Chemical: sodium borohydride, ethanol, methanol, toluene, N,N-dimethylformamide (DMF), dimethyl sulfoxide (DMSO), citric acid, acetic acid, sodium hydroxide, cesium hydroxide. Silver nitrate and 4-mercaptophenol were purchased from Sigma-Aldrich. Gold (III) chloride was synthesized in-house dissolving gold ingot in aqua regia. The p-MBA was purified by selective dissolution and recrystallization. All other reagents were used without further purification. De-ionized water (18.2 M $\Omega$  cm) was used.

### 2.2.2 Synthesis of $M_4Au_xAg_{44-x}(p-MBA)_{30-y}(SC_6H_4OH)_y$ by Galvanic Exchange

The galvanic exchange reactions of  $M_4Ag_{44}(p-MBA)_{30}$  with Au-  $SC_6H_4OH$  were carried out in DMF, where  $SC_6H_4OH$  corresponds to 4-mercaptophenol with a deprotonated thiol group. The molar ratios of  $M_4Ag_{44}(p-MBA)_{30}$  and gold-thiolate used were 1:1, 1:3, 1:6, 1:12, 1:18, 1:24 and 1:44, respectively. A stock solution of  $M_4Ag_{44}(p-MBA)_{30}$  was prepared as described elsewhere.<sup>11, 77</sup> The concentration of the stock solution was determined using the molar absorption coefficient of  $M_4Ag_{44}(p-MBA)_{30}$ .<sup>77</sup> The gold thiolates and  $M_4Ag_{44}(p-MBA)_{30}$  solutions were mixed according to the above-mentioned ratios for the galvanic exchange reactions. The reactions were monitored by using UV-visible absorption spectroscopy and mass spectrometry.

### 2.2.3 Synthesis of gold thiolate

A stock solution of gold-thiolate was prepared by reacting a 1:3 molar ratio of  $\text{HAuCl}_4 \cdot 3\text{H}_2\text{O}$  and 4-mercaptophenol in water/DMSO solvent (7:4 by volume). The reaction mixture was sonicated for 5 min and stirred for 5 min. An insoluble mass of gold thiolate formed and segregated out of the solvent, which was later solubilized by adding an aqueous cesium hydroxide solution (50% by weight). Cesium hydroxide raised the pH to  $\sim 10$ , which deprotonated the carboxylic acid group present in the thiol ligand and made the gold thiolate soluble in polar solvents. 1200  $\mu\text{L}$  of acetic acid was added in order to protonate the thiol ligands and precipitate the gold thiolate out of the solvent. At this point, the reaction mixture was centrifuged, and the supernatant was discarded. The sediment was re-dissolved in highly basic water/DMSO solvent (7:4 by volume,  $\text{pH}=12$ ). The gold thiolate was precipitated again out of the solvent by adding 1 mL of concentrated nitric acid. The reaction mixture was centrifuged, and the supernatant was discarded. The process of dissolution of gold thiolate with cesium hydroxide solution and precipitation with acetic acid was done twice to remove unreacted materials and residual ions. The final supernatant obtained was free of  $\text{Au}^{3+}$  and  $\text{Cl}^-$ .

The gold thiolate precipitate was dissolved in neat DMF. The calibration curves of gold-thiolate solutions, based on phenyl ring absorbance at  $\sim 308$  nm versus concentrations, were plotted and used for quantifying the number of gold thiolates. Thus, a prepared gold-thiolate solution was used as a stock solution for reacting with the solution of  $\text{M}_4\text{Ag}_{44}(\text{p-MBA})_{30}$  nanoparticles.

### 2.2.3 Optical measurements

Optical absorption spectra were recorded on a Perkin Elmer Lambda 950 spectrophotometer. Spectra of  $M_4Au_xAg_{44-x}(p-MBA)_{30-y}(SPhOH)_y$  were measured in neat DMF solvents. For samples made by galvanic exchange reaction, solutions were centrifuged and diluted 40 times to 2 mL and measured in a 5 mm cuvette.

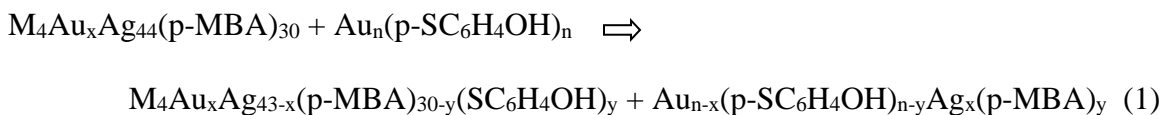
### 2.2.4 Electrospray ionization mass spectrometry

High-resolution mass spectrometry data were collected on a Synapt HDMS G1 quadrupole time-of-flight ion mobility mass spectrometer equipped with a nanoflow electrospray ionization source (Waters Corp.) using homemade fused silica emitters. All mass spectra were collected in negative V-mode. The following instrumental parameters were used during data acquisition: capillary voltage, 2.0–4.0 kV; sampling cone, 7–20V; extraction cone, 4.0 V; cone gas, 0 L/h; nanoflow; trap collision energy, 0.5 V; transfer collision energy, 1.0 V; source temperature, 40 °C; desolvation temperature, 120 °C. The external calibration of the instrument was done in negative ion mode using cesium iodide in the range of  $100 \leq m/z \leq 5000$ . Data were collected and processed using MassLynx 4.1 software (Waters Corp.). Isotopic patterns were simulated using mMass 5.5 freeware (copyright, Martin Strohm). All samples were dissolved in DMF with a concentration of approximately 2.5 mg/mL. For sample preparation of galvanic exchange experiments, 300  $\mu$ L of each sample were precipitated by 350  $\mu$ L of DMF. Precipitates were collected by centrifugation at 5000 RCF for 30 s. Isolated nanoparticles were protonated in 300  $\mu$ L of DMF three times following precipitation with toluene and centrifugation. The first protonation was carried out by adding approximately ~20 crystals of citric acid and the

second and third protonation were each carried out by adding 20  $\mu\text{L}$  of formic acid. After the third protonation, NPs were cleaned by one more precipitation-dissolution cycle with no additives. Final samples were centrifuged at 16000 RCF for 2 min to get rid of any insoluble material prior to ESI-MS analysis.

## 2.3 Results and Discussion

Murray's group showed the efficiency of galvanic exchange reactions when using metal-ligand complexes over the metal salts as reactants.<sup>69</sup> In the present study, monometallic  $\text{M}_4\text{Ag}_{44}(\text{p-MBA})_{30}$  nanoparticles can be transformed into bimetallic as well as surface-modified  $\text{M}_4\text{Au}_x\text{Ag}_{44-x}(\text{p-MBA})_{30-y}(\text{SC}_6\text{H}_4\text{OH})_y$  nanoparticles by their reaction with metal-thiolate species, which contains the gold and 4-mercaptophenol. The transformation of  $\text{M}_4\text{Ag}_{44}(\text{p-MBA})_{30}$  into  $\text{M}_4\text{Au}_x\text{Ag}_{44-x}(\text{p-MBA})_{30-y}(\text{SC}_6\text{H}_4\text{OH})_y$  by galvanic exchange occurred as step wise reactions between gold-thiolate polymers. Each sequential reaction involves the substitution of one gold atom for one silver atom and substitution of one p-MBA ligand to one  $\text{HSC}_6\text{H}_4\text{OH}$  ligand. The general equation for any reaction can be written as follows.



where  $0 < x < 12$  and where  $0 < y < 3$ . The  $\text{Au}_n(\text{p-SC}_6\text{H}_4\text{OH})_n$  and  $\text{Au}_{n-x}(\text{p-SC}_6\text{H}_4\text{OH})_{n-y}\text{Ag}_x(\text{p-MBA})_y$  represent the metal thiolates before and after the exchange reaction, respectively.

Galvanic exchange reactions were carried out in DMF and were incubated for 24 hours in the freezer. A series of spectra shows the evolution of the exchanged species as a function of time. As shown in Figure 2-1, after 24 hours the optical spectra did not change significantly, suggesting that equilibrium was already reached.

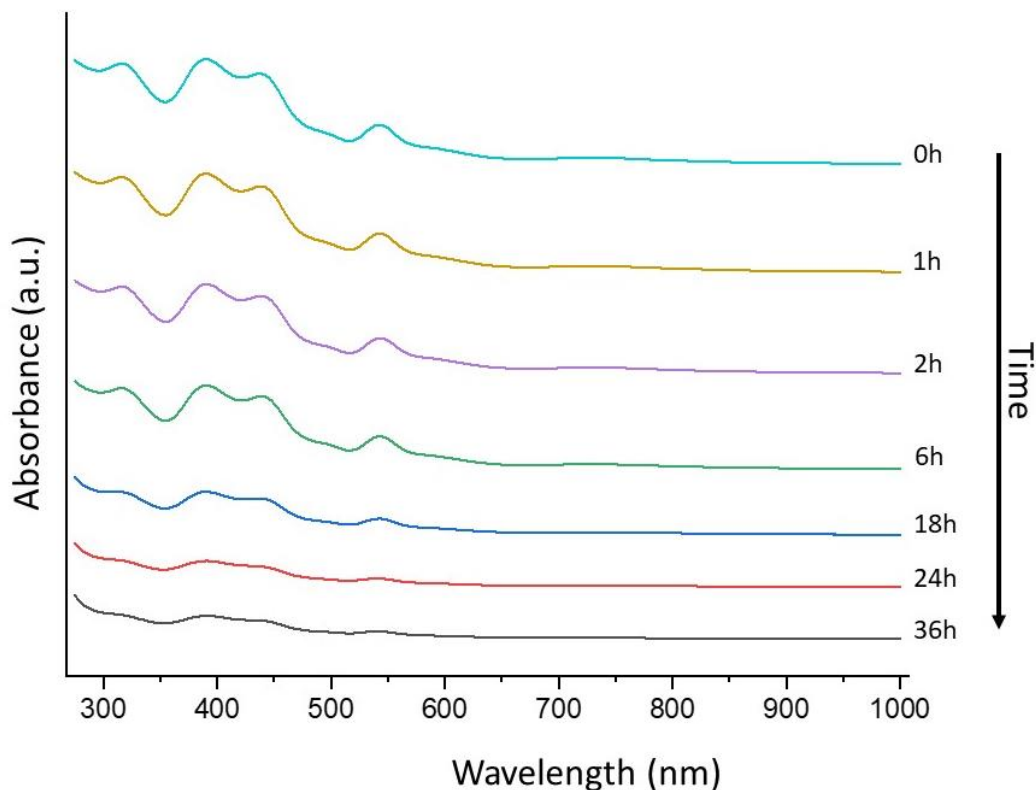


**Figure 2-1.** Optical absorption spectra of  $M_4Au_xAg_{44-x}(p-MBA)_{30-y}(SC_6H_4OH)_y$  species synthesized with a 1:44 input ratio of Ag44: Au-(SC<sub>6</sub>H<sub>4</sub>OH) as a function of time. Absorbances were not adjusted but spectra were offset for clarity.

per  $M_4Ag_{44}(p-MBA)_{30}$  MPC. For example, for a reaction mixture that contained one gold atom for one silver atom, the input ratio would be 1:44. The distribution of exchange as a function of input ratio shown in figure 2-2.

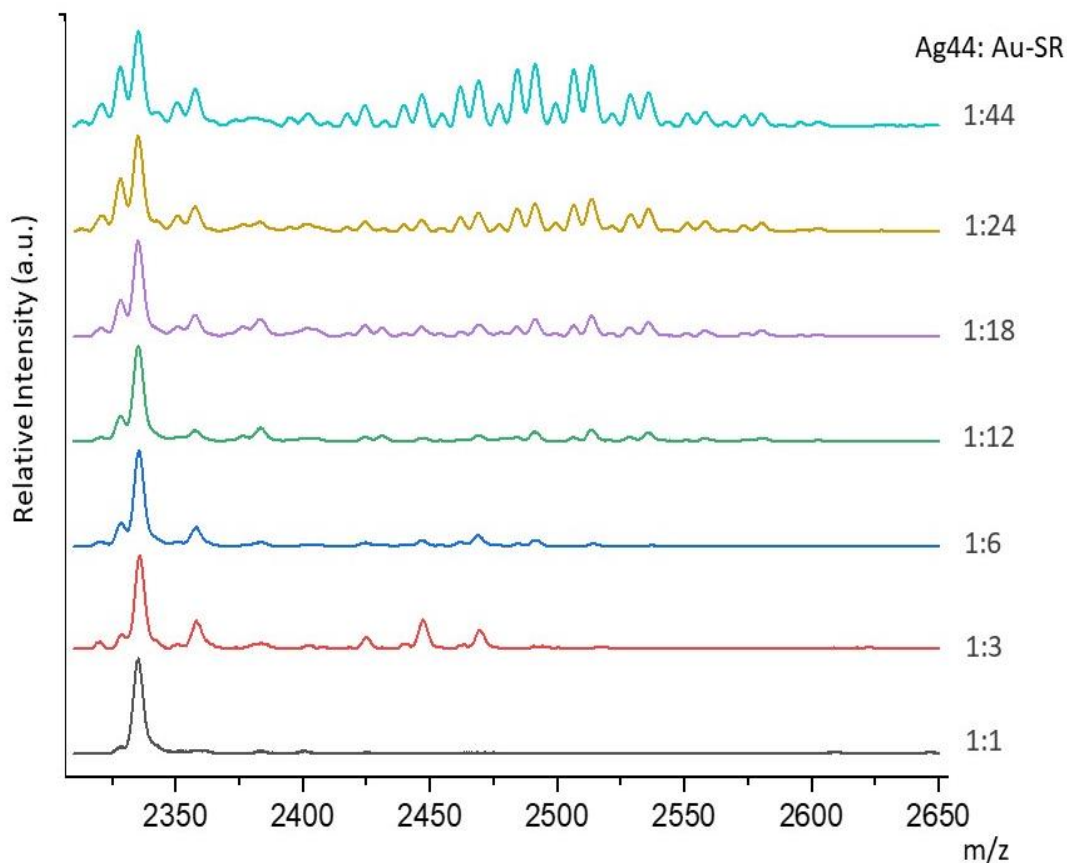


**Figure 2-2.** ESI-MS spectra showing the distribution of  $M_4Au_xAg_{44-x}(pMBA)_{30-y}(SC_6H_4OH)_y$  species synthesized by galvanic exchange using different  $M_4Ag_{44}(pMBA)_{30}:Au-(SC_6H_4OH)$  input ratios.

ESI-MS analysis of galvanic exchange reactions' product distributions showed complex patterns of peaks for both metal and ligand substitutions. The highest intense peak to the left in each distribution corresponds to the zero-metal exchange. For clarity and to interpret the results clearly, the ESI-MS spectra were stacked and rescaled as in figure 2-3.

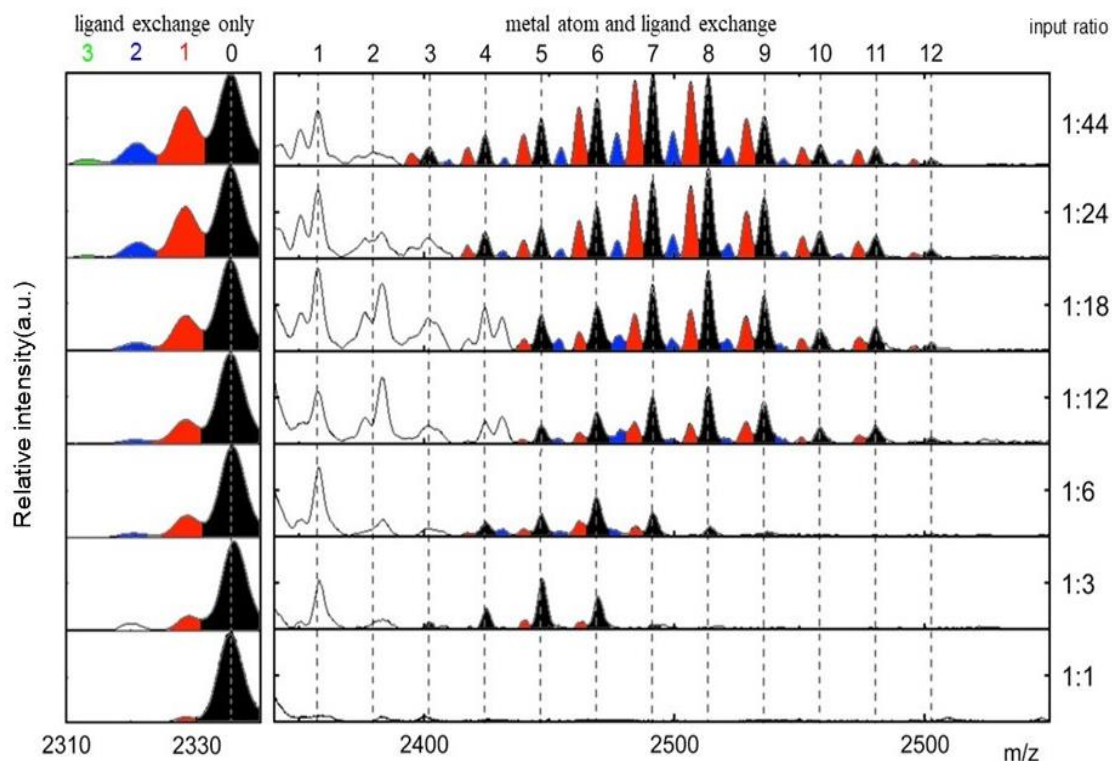


**Figure 2-3.** Rescaled ESI-MS spectra showing distribution of  $M_4Au_xAg_{44-x}(pMBA)_{30-y}(SPhOH)_y$  species synthesized by galvanic exchange using different  $M_4Ag_{44}(pMBA)_{30}:Au-(SC_6H_4OH)$  input ratios. Peaks correspond to 0 ligands exchanged, 1 ligand exchanged, 2 ligands exchanged, and 3 ligands exchanged species colored in black, red, blue and green, respectively.

The panel to the left in figure 2-2 shows zero (0) metal atom substitution with ligand exchange. The extent of the ligand substitution increased as the gold-polymer concentration increased. The masses of  $SC_6H_4OH$  and p-MBA are 125.18 Da and 153.19 Da, respectively. Therefore, substitution of p- $SC_6H_4OH$  for p-MBA would decrease the mass of  $Ag_{44}(pMBA)_{30}$  by 28.01 Da (7 m/z for the 4- ion). This mass difference corresponds to the observed peak spacing towards the lower m/z range. Maximum ligand substitution is limited to 3 ligands. The data confirmed that the gold thiolate is carefully

cleaned with no free ligands, and the ligand substitution can be attributed to the gold thiolate.

There are three possible species that correspond to the observed peak patterns in the panel to the right in figure 2-3: (i) zero ligand-exchanged species (black), (ii) species with one ligand exchange (red), and (iii) two ligand exchanged species (blue). Each product distributions shift towards the higher  $m/z$  range with increasing input ratio up to 1:12, and distributions become stable from 1:12 to 1:44 input ratio (see black peaks in Fig. 2-2). The input ratio did not match with the average number of gold atom substitution. The product distributions of galvanic exchange with heteroligand metal complex (Au-  $SC_6H_4OH$ ) are different from those of homoligand metal complex (Au-pMBA) as well as co-reduction reactions. But the substitution was limited to 12 gold heteroatoms, as in the galvanic exchange with Au-pMBA as well as co-reduction reaction. All the metal only exchanged product distributions were fitted with Gaussian functions (see Figure 2-4), confirming random substitution.

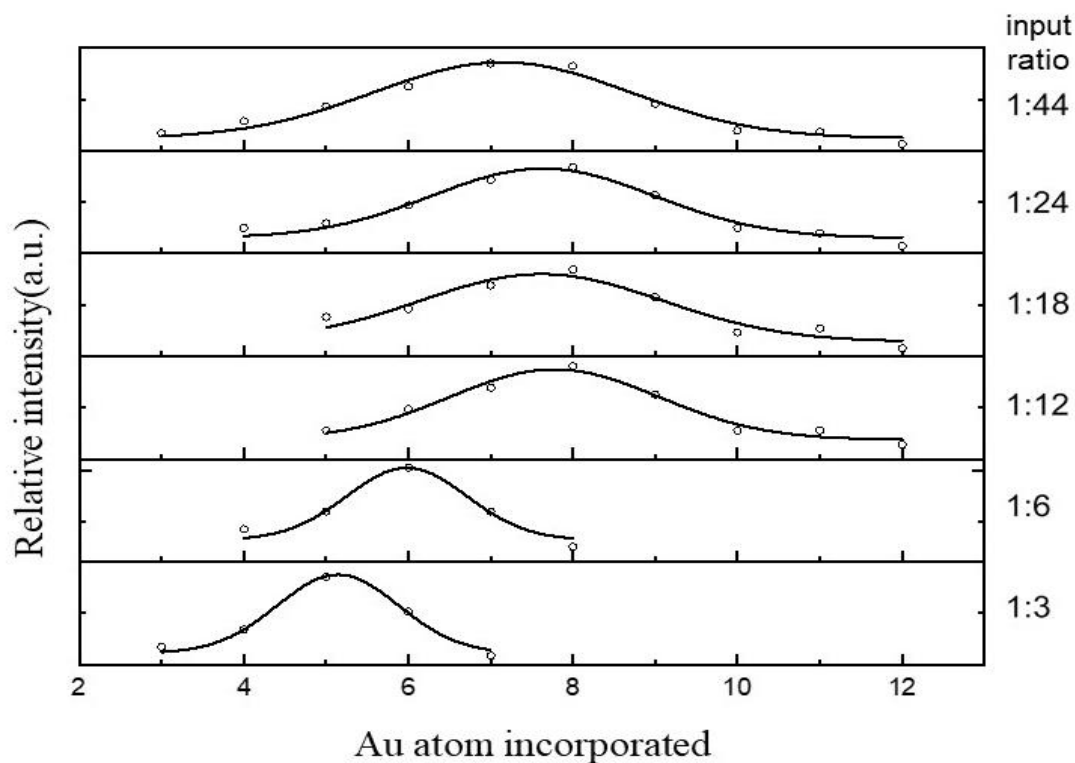


**Figure 2-4.** Gaussian fits to metal atom substituted peak distributions.

Both one ligand (red peaks) and two ligands (blue peaks) follow similar distributions to the metal only substitution. For both cases, the average number of substitutions increased with an increasing input ratio up to 1:12. Then the distributions shifts stop and increase uniformly up to 1:44 input ratio. Both one ligand and two ligand product distributions were fitted with Gaussian functions (see figure 2-5, 2-6), confirming random substitution. Three ligands (green peaks) substitution only appear for high input ratios visible next to the zero metal substituted peaks. In the rest of the distributions three ligand peaks are not visible due to the peak overlap and the low intensity.

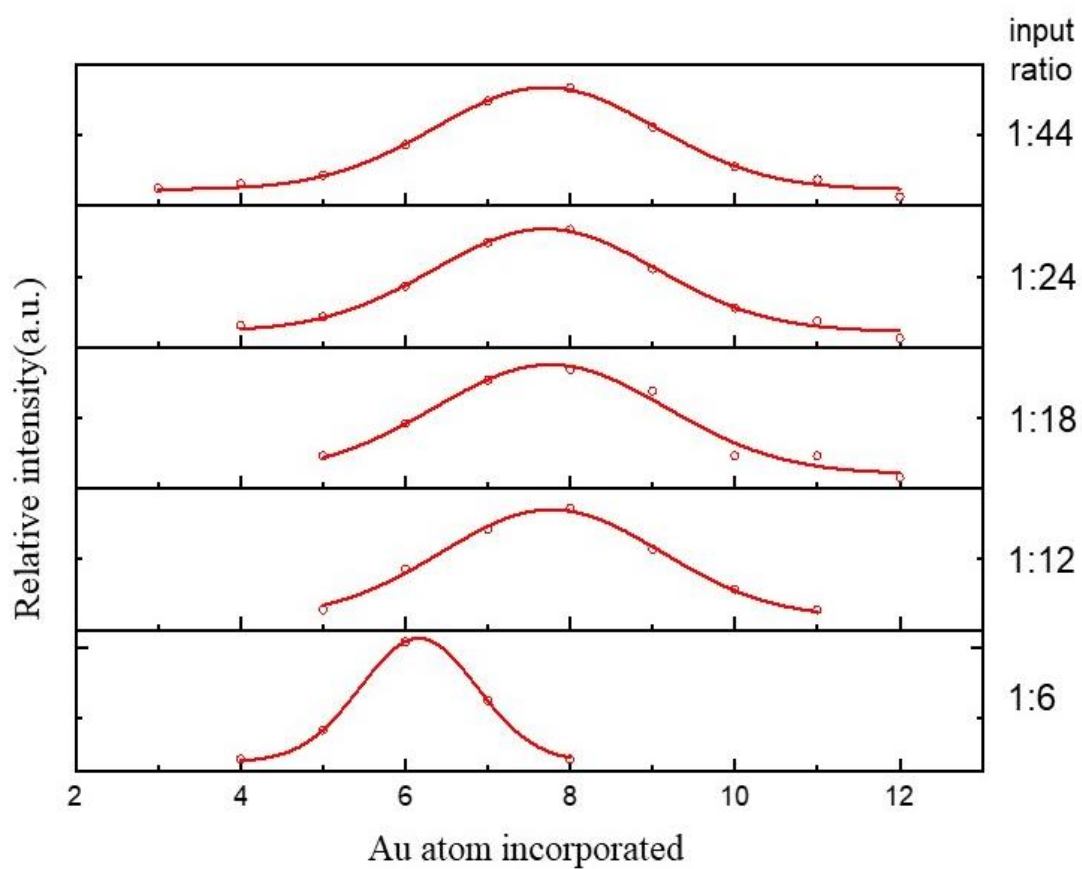


**Figure 2-5.** Gaussian fits to metal atom exchange with one ligand

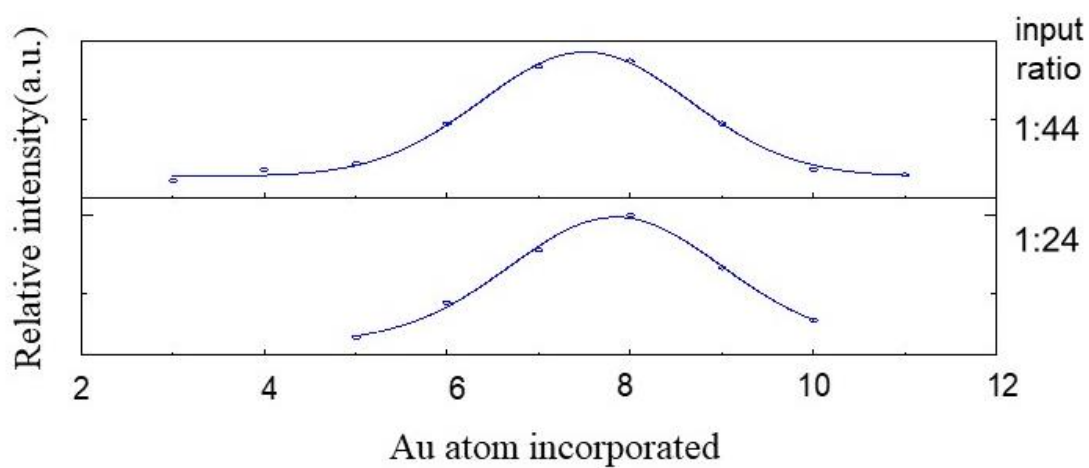


**Figure 2-6.** Gaussian fits to metal atom exchange with two ligands

All the distributions with only metal substitution, one ligand substitution, and two ligand substitutions fit with Gaussians. That confirmed the metal atom substitutions and ligand substitutions are independent of one another. However, both the gold atom and ligand are parts of the same reactant molecule. It is, therefore, surprising that gold atom substitution and ligand substitutions are uncorrelated. Also, galvanic exchange with metal atom alone was found to be less efficient than metal-ligand complex, which suggests possible ligand role in metal exchange reactions. Metal atom exchange mechanism likely involves ligands, but those ligands remain where they came from, either in the ligand complex or on the cluster. According to the metal atom and ligand substitution patterns, it's clear that metal is much more efficient in substitution than ligand, but it is not clear if they are determined by thermodynamics or kinetics.

## **2.4 Conclusions**

According to the metal atom and ligand substitution patterns, it's clear that metal is much more efficient in substitution than ligand, but it is not clear if they are determined by thermodynamics or kinetics. Metal atom substitution is strongly preferred over ligand substitution, possibly due to stronger electrophilicity of Au or due to kinetic barriers. No correlation was found between heteroatom and ligand substitution, even though metal atom substitution involves ligands in some way. Metal atom exchange mechanism likely involves ligands, but those ligands remain where they came from, either in the ligand complex or on the cluster. Metal substitution and ligand substitution reaction mechanisms are independent and different. In each reaction, either a metal atom is substituted, or a ligand is substituted, not both together.

## Chapter 3

### Ligand exchange reactions of MPCs

#### 3.1. Introduction

Ligand-exchange reactions on MPCs<sup>50, 87-88</sup> are widely used as a principal mode of modification and functionalization of nanoparticles. Ligand exchange reactions are important to modify the optical,<sup>89</sup> electronic,<sup>90</sup> and structural properties<sup>91</sup> of thiolate MPCs. It is also possible to modify MPCs to perform specific tasks such as photosensitivity<sup>60</sup> and molecular recognition.<sup>92</sup> Moreover, most MPCs are synthesized with protective ligands and solvents that are not usable for applications. In such a situations ligand exchange becomes a crucial post-synthetic modification technique for tuning surface properties. Also, these ligand exchange reactions have recently been used for size-selective synthesis can be used as a method to get monodisperse products of MPC where direct synthetic methods lead to polydisperse products distributions.<sup>93-94</sup>

These ligand substitution reactions have been widely studied for the exchange site in gold MPCs, mainly using nuclear magnetic resonance spectroscopy and mass spectrometry as the main characterization techniques.<sup>87, 95-96</sup> Other techniques such as single-crystal X-ray diffraction structure analysis,<sup>97-98</sup> reversed-phase high-performance liquid chromatography (RP-HPLC), and theoretical techniques such as density functional theory calculations,<sup>99-100</sup> have also been used for the understanding of ligand substitution reactions.

Ackerson and co-workers identified the preferable ligand-exchange sites on  $\text{Au}_{102}(\text{p-MBA})_{44}$ .<sup>98</sup> Based on x-ray crystal structure measurements, they found that the incoming p-bromothiophenol ligands first attack top or bottom sites along the  $C_5$  axis of the clusters. Out of the 22 possible symmetric ligand sites on the cluster, only these two sites were found to be partially exchanged with the incoming ligands during a fast 5 min exchange reaction, confirming those two sites are kinetically favorable for ligand exchange to occur. The site preference can be explained by the solvent accessibility of the involved surface Au atoms and is further supported by DFT calculations with a detailed mechanistic pathway.<sup>98</sup>

The same group used a small nanocluster of  $\text{Au}_{25}(\text{SR})_{18}$  to determine initial exchange sites.<sup>97</sup> Two oppositely distributed ligands[[I don't know what this means]] were found to exchange incoming ligands, confirming site-specificity. The involved gold atoms were found to be more accessible to the solvent, consistent with the previous study.<sup>98</sup> Theoretical studies by Aikens and co-workers found that the terminal-ligands and staple gold atoms were favorable sites for ligand exchange.<sup>99</sup> Also, the Negishi group reported a specific site preference in ligand exchange reactions of  $\text{PdAu}_{24}(\text{SR})_{18}$  with a different isomeric form of the ligand.<sup>101</sup>

Although many studies have been carried out to functionalize and modify gold MPCs, less attention has been paid to the Ag MPCs.<sup>102</sup> Among  $\text{Ag}_n(\text{SR})_m$  clusters, the  $\text{M}_4\text{Ag}_{44}(\text{p-MBA})_{30}$  nanoparticle (see Figure 3-1a) is a promising model system for studying the chemistry of MPCs since it is a well-defined and well-studied system that can act as a molecular laboratory to investigate a variety of basic questions regarding the

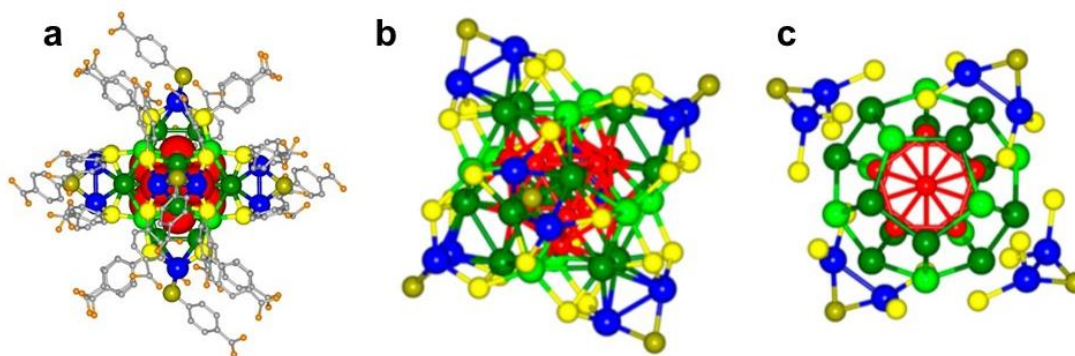


**Figure 3-1.** Structure of a  $\text{Na}_4\text{Ag}_{44}(\text{p-MBA})_{30}$  mNP. (a) Complete structure showing silver core and *p*-MBA ligands. (b) Six  $\text{Ag}_2\text{S}_5$  units cap the dodecahedral core to complete the inorganic structure. (c) An alternative view of the  $\text{Ag}_2\text{S}_5$  mounts, separated from the dodecahedral  $\text{Ag}_{32}$  core. Color scheme: gray, carbon; orange, oxygen; blue, exterior silver atoms in the mounts; gold, bridging sulfur atoms in the mounts. Reproduced with permission from reference 1. Copyright 2013 Nature Publishing Group.

ligand exchange process: site-specificity of the substitution, the extent of the substitution, and nature of the substitution.

The inner core of  $\text{M}_4\text{Au}_{44}(\text{pMBA})_{30}$  is composed of the 12 atoms innermost icosahedral shell surrounded by 20 atoms in a dodecahedral outer shell. The core is surrounded by six octahedrally-arranged  $\text{Ag}_2(\text{SR})_5$  capping mounts. Each of these mounts contains 2 Ag atoms and 5 ligands. Each mount has 4 chemically equivalent ligand positions at the base and one additional bridging ligand position on top. The bridging position is a more accessible position to incoming ligands to substitute.

In this study,  $[\text{Au}_{44}(\text{p-MBA})_{30}]^{4-}$  was used to study the ligand exchange with *p*-mercaptophenol (SHPhOH), *p*-fluorothiophenol, (4-FTP), *p*-chlorothiophenol (4-CPT), *p*-bromothiophenol (4-BTP) as ligands to probe questions mentioned above.

## 3.2 Experimental

### 3.2.1 Chemicals

Silver nitrate ( $\text{AgNO}_3$ ), 4-mercaptobenzoic acid (p-MBA, technical grade, 90%), 4-mercaptophenol (97%), 4-fluorothiophenol (4-FTP, 98%), 4-chlorothiophenol (4-CTP, 97%), 4-bromothiophenol (4-BTP, 95%), 2-bromothiophenol (2-BTP, 97%), N,N-dimethylformamide (DMF, 99%), dimethyl sulfoxide (DMSO, 99%), cesium hydroxide ( $\text{CsOH}$ , 50% w/w solution), citric acid (ACS reagent,  $\geq 99.5\%$ ) and toluene (anhydrous, 99.8%) were purchased from Sigma Aldrich. The pMBA was purified by selective dissolution in methanol. All other chemicals were used without further purification. De-ionized water ( $18.2 \text{ M}\Omega \text{ cm}$ ) was used.

### 3.2.2 Ligand exchange on $\text{M}_4\text{Ag}_{44}(\text{p-MBA})_{30}$ using 4-HSC<sub>6</sub>H<sub>4</sub>OH, 4-FTP, 4-CTP and, 4-BTP.

The ligand exchange reactions of  $\text{M}_4\text{Ag}_{44}(\text{p-MBA})_{30}$  with all ligands were carried out in DMF. A stock solution of  $\text{M}_4\text{Ag}_{44}(\text{p-MBA})_{30}$  was prepared as described elsewhere.<sup>11, 77</sup> The concentration of the stock solution was determined using the molar absorption coefficient of  $\text{M}_4\text{Ag}_{44}(\text{p-MBA})_{30}$ .<sup>77</sup> The stock solutions of each ligand were prepared in DMF (0.05M). The molar ratios of  $\text{M}_4\text{Ag}_{44}(\text{p-MBA})_{30}$  and 4-HSC<sub>6</sub>H<sub>4</sub>OH/4-FTP used were 1:1, 1:6 and, 1:12 and only 1:1 ratio was used with other ligands. The  $\text{Ag}_{44}$  and ligand solutions were mixed in the above-mentioned ratios and the resulting mixtures were vortexed vigorously, incubated in the freezer for 6 hours. The ligand exchange reactions were monitored by using UV-visible absorption spectroscopy and mass spectroscopy.

### **3.2.4 Electrospray ionization mass spectrometry (ESI-MS)**

High resolution mass spectrometry data were collected on a Synapt HDMS G1 quadrupole-time-of-flight ion mobility mass spectrometer equipped with a nanoflow electrospray ionization source (Waters Corp.), using homemade fused silica emitters. All mass spectra were collected in negative V-mode. Following instrumental parameters were used during data acquisition : capillary voltage, -2.0–4.0 kV; sampling cone, 7–20V; extraction cone, 4.0 V; cone gas, 0 L/h; nanoflow, 0.1 bar; trap collision energy, 0.5 V; transfer collision energy, 1.0 V; source temperature, 40 °C; desolvation temperature, 120 °C. The external calibration of the instrument was done in negative mode using cesium iodide in the range of  $100 \leq m/z \leq 5000$ . Data were collected and processed using MassLynx 4.1 software (Waters Corp.). The sample preparation was carried out by taking an aliquot from the reaction mixture, centrifuging out any solid particles and diluting the supernatant with the DMF to the optimal concentration.

## **3.3 Results and Discussion**

### **3.3.1 Preferential exchange sites**

The ligand exchange reaction was performed by reacting  $[\text{Au}_{44}(\text{p-MBA})_{30}]^4$  and 4-SHPhOH and 4-FTP in DMF. The molar ratios of cluster to ligand were set to 1:1, 1:6 and 1:12 to determine the exchange site in low ligand-exchanged products. After 6 h of reaction, the excess ligands and insoluble byproducts were removed from the mixture.

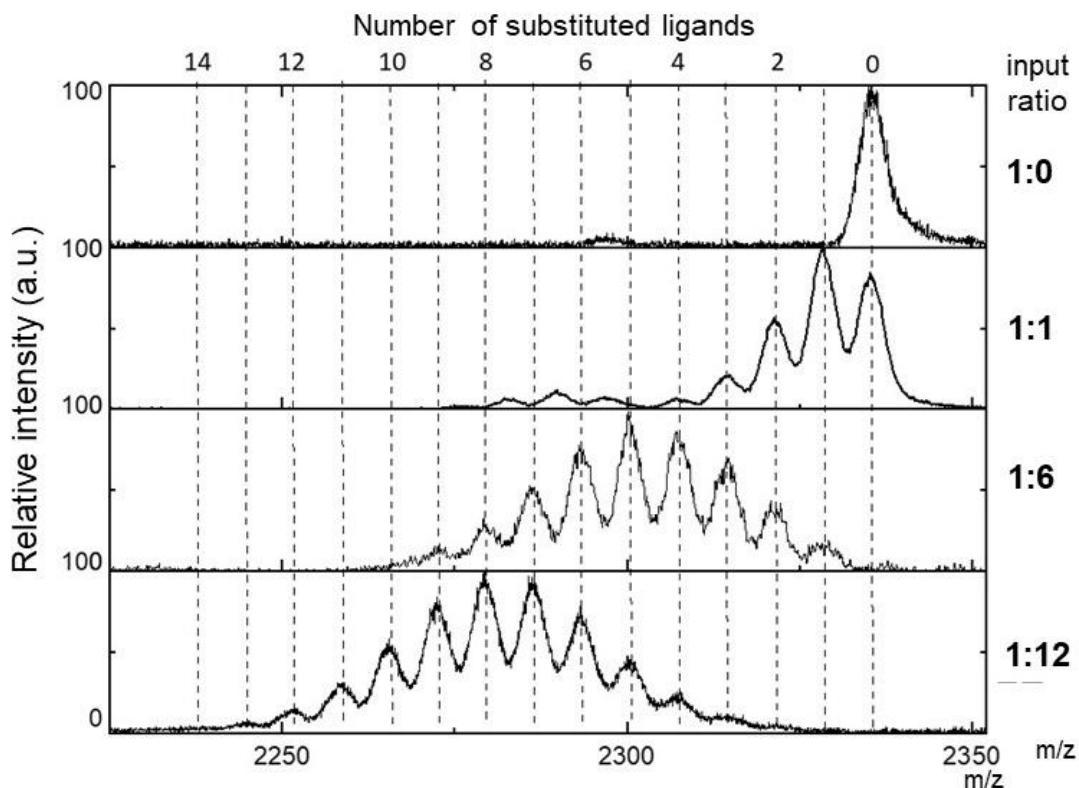


**Figure 3-2.** Negative-ion ESI mass spectra of the products prepared by reaction of  $\text{Na}_4\text{Au}_{44}(\text{p-MBA})_{30}$  with 4-HSC<sub>6</sub>H<sub>4</sub>OH in DMF at different input ratios.

Figures 3-2 and 3-3 show ESI mass spectra of product distributions of ligand exchange of  $\text{Na}_4\text{Au}_{44}(\text{p-MBA})_{30}$  between 4-HSC<sub>6</sub>H<sub>4</sub>OH and 4-FTP respectively. Peaks were ascribed to  $[\text{Au}_{44}(\text{p-MBA})_{30-x}(\text{4-HSC}_6\text{H}_4\text{OH})_x]^{4-}$  ( $x = 1$  to 13) and  $[\text{Au}_{44}(\text{p-MBA})_{30-x}(\text{4-FTP})_x]^{4-}$  ( $x = 1$  to 16). The results confirm that ligand exchange occurred in both reactions, with the number of substituting ligands increased with increasing input ratio. In both ligand exchange reactions, less intense peaks can be observed around 2300 m/z. These peaks correspond to the species produced from  $[\text{Ag}_{44}(\text{p-MBA})_{29}]^{4-}$ . Similar results were obtained for both ligands, and both product distributions are random toward higher input ratios.

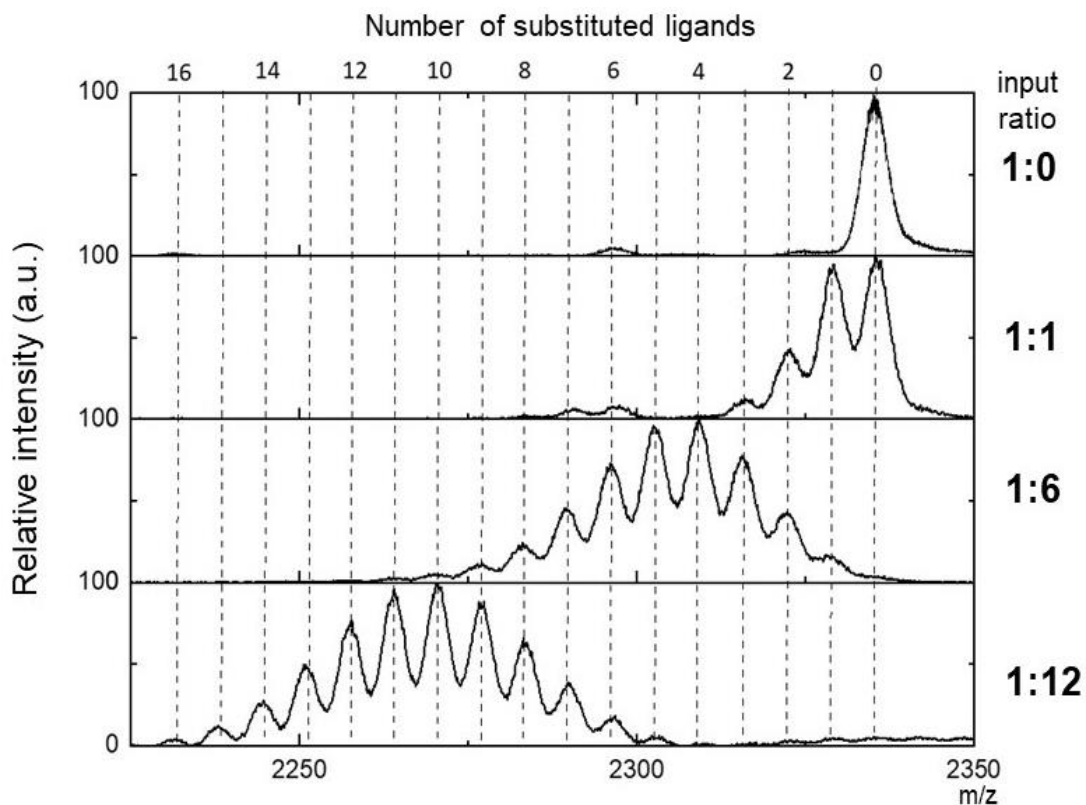


**Figure 3-3.** Negative-ion ESI mass spectra of the products prepared by reaction of  $\text{Na}_4\text{Au}_{44}(\text{p-MBA})_{30}$  with (4-FTP) in DMF at different input ratios.

This indicates that ligand substitution, either random or possible internal rearrangement after substitution. The bridge position may act as an entry point to the incoming ligands, and once substituted, ligands may move to the base positions leaving the bridge position open for the next substitution. Both ligands exhibit similar characteristics. The substitutions are often close but less than the input ratio for both ligands. Therefore, the extent of reactions  $<1$ , and both reactions are product favored.

### 3.3.2 Nature of the substitution

This study focused on the ligand exchange of  $\text{Ag}_{44}$  with halogen (F, Cl, Br) substituted thiophenols. All thiophenols used were para-substituted, to minimize possible steric effects. Halogenated thiophenols are one of the simplest model systems to study the electronic nature of the ligand substitution as they contain electronically different substituents (F, Cl and, Br) with a common aromatic moiety. Investigation of the nature of the substitution of the ligand as a function of that substituent's electron induction ability offers insight into how the electronic nature of the ligand determines the extent of the reaction process. The halogens follow induction order as  $\text{F} > \text{Cl} > \text{Br}$  based on their electronegativity and the reactivity of ligands should vary according to that order. To test the hypothesis 1:1 ligand exchange between  $\text{Ag}_{44}$  and halogens substituted thiophenols were carried out.

Figure 3-4 shows ESI mass spectra of product distributions from ligand exchange reactions of  $\text{M}_4\text{Au}_{44}(\text{p-MBA})_{30}$  with 4-FTP, 4-CTP, and 4-BTP, all of which were carried out under the same reaction conditions. Peaks in each spectrum were ascribed to  $[\text{Au}_{44}(\text{p-MBA})_{30-x}(4\text{-FTP})_x]^{4-}$  ( $x = 1$  to 3),  $[\text{Au}_{44}(\text{p-MBA})_{30-x}(4\text{-CTP})_x]^{4-}$  ( $x = 1$  to 6) and  $[\text{Au}_{44}(\text{p-MBA})_{30-x}(4\text{-BTP})_x]^{4-}$  ( $x = 1$  to 4), respectively. This confirms that ligand exchange occurred in all three reactions and that those exchange reactions occurred to different extents. The greatest extent of the reaction was exhibited by 4-CTP with 6 exchanged ligands and 4-FTP was the lowest with 3 exchanged ligands. The results clearly do not follow the induction order of the halides, which was contrary to expectations. This indicates that induction alone does not account for the reactivity of the ligands toward substitution into  $\text{M}_4\text{Au}_{44}(\text{p-MBA})_{30}$ .

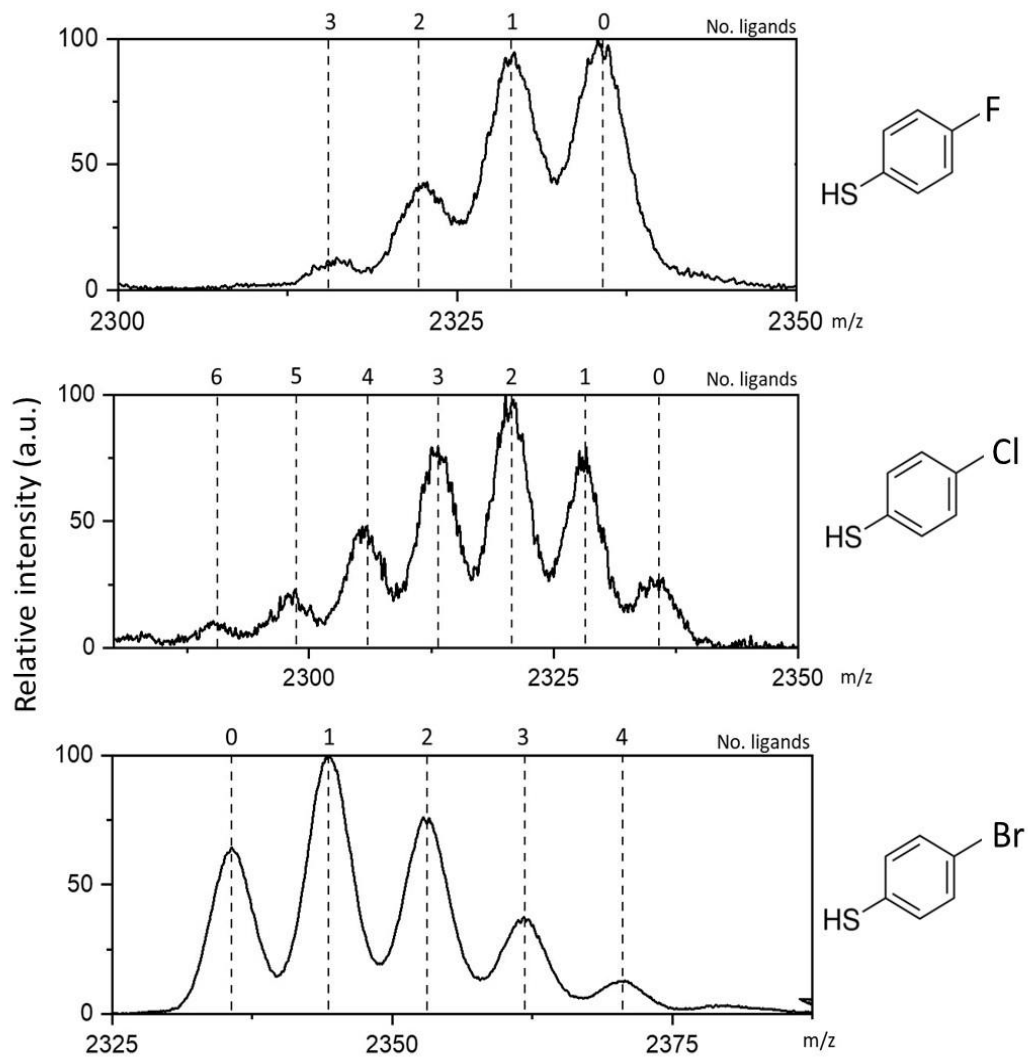


**Figure 3-4.** Negative-ion ESI mass spectra of the products prepared by reaction of  $M_4Au_{44}(p-MBA)_{30}$  with 4-FTP, 4-CTP and 4-BTP in DCM at 1:1 input ratio.

4-FTP behaves differently in comparison to the other halogenated thiophenols (4-CTP, 4-BTP), wherein it is much less reactive than would be expected based upon induction alone and the assumption of an electrophilic substitution mechanism. This anomalous observation can be explained using theoretical and mechanistic models. Fluorobenzene exhibits both inductive electron withdrawal from the benzene ring and  $\pi$  electron donation (mesomeric effect) to the benzene ring at the same time. The

mesomeric (resonance) effect is much stronger for fluorine than for other halogens (Cl, Br) and acts as an activation group rather than inductively pulling electron density from the phenyl ring.

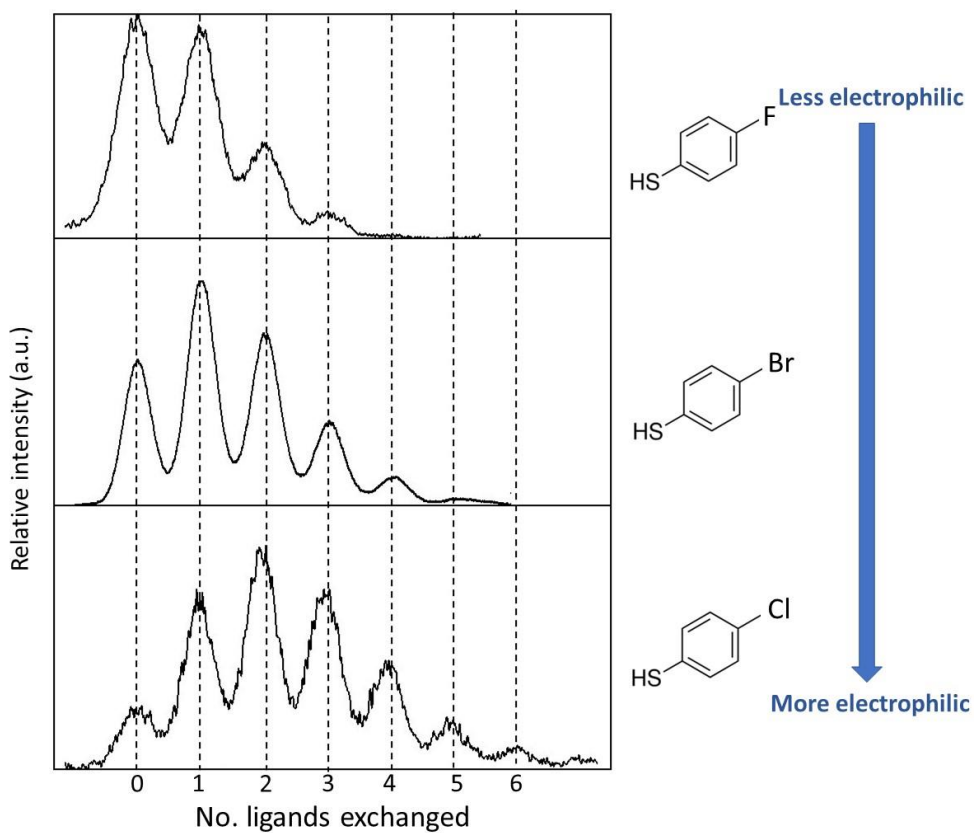


**Figure 3-5.** Negative-ion ESI mass spectra of the products prepared by reaction of  $M_4Au_{44}(p-MBA)_{30}$  with 4-FTP, 4-CTP and, 4-BTP in DCM at 1:1 input ratio arranged according to extent of the reaction (4-CTP and 4-FTP axes are reversed; all are rescaled such that the abscissa corresponds to the number of ligands substituted).

By considering the net impact of both induction and mesomeric effect, the activity can be rearranged as  $F < Br < Cl$ . Measurements of the extent of ligand substitution agree with this order (see Figure 3-5), with a maximum of  $\sim 3$  ligands exchanged for 4-FTP, 4 or 5 ligands exchanged for 4-BTP, and 6 or 7 ligands exchanged for 4-CTP. From the correspondence between the extent of ligand substitution and the electrophilicity of the

ligands, based on the electron-withdrawing nature and mesomeric effect of the ring substituents, it can be concluded that the ligand substitution in  $\text{Ag}_{44}$  is electrophilic in nature.

### 3.4 Conclusions

The site preference of ligands during ligand substitution reactions, extent of the substitution and the nature of the ligand exchange reactions were investigated using the model system,  $\text{M}_4\text{Ag}_{44}(\text{p-MBA})_{30}$ . The study shows random substitution for both ligands (4-HSC<sub>6</sub>H<sub>4</sub>OH and 4-FTP) confirming no final site preference for ligands on  $\text{M}_4\text{Ag}_{44}(\text{p-MBA})_{30}$  cluster. It was found that the average number of substitutions for both ligands are close but less than the input ratio. Also, both exchange reactions were found to be product-favored. The ligand substitution reactions on  $\text{M}_4\text{Ag}_{44}(\text{p-MBA})_{30}$  were found to be electrophilic in nature.

## Chapter 4

### Conclusions

Monolayer protected clusters (MPCs) have received great research interest due to their potential applicability in various fields, including optoelectronics, biomedicine, catalysis, and photochemistry. The field of metal MPCs has significantly advanced with Brust et al.'s pioneering work in the synthesis of small metal nanoparticles in the early 1990s. Back then, the synthesis and characterization of new MPCs received greater interest. Even today, researchers work extensively in the synthesis and characterization of new clusters. So far, various clusters have been reported with successful formulae determinations and crystal structures.

Despite the significant achievements in synthesis and structural determinations, the molecular level understanding of reactivity and post-synthetic modification of these materials is still lacking. It is crucial to study and understand different aspects of these MPCs to use them in applications. Post synthetic functionalization and modifications of MPCs are important considerations for their intended application. Mainly there are two modes of functionalization: heteroatom substitution or heteroligand substitution.

The studies of Ag MPCs have lagged behind the gold analogs due to their high reactivity and susceptibility to oxidation and aggregation. Despite that, Ag MPCs are expanding their roles in many areas due to desirable optical and electronic properties. In

this study, we have presented experimental results for basic functionalization reactions on  $\text{Ag}_{44}$  as an important step towards the goal of understanding their post-synthetic chemistry.

First, bimetallic and surface functionalized nanoparticles were synthesized by galvanic exchange using a complex composed of both a heterometal (Au) and a heteroligand (4-HSC<sub>6</sub>H<sub>4</sub>OH). Nanoparticles with up to 12 substituted Au atoms were found in the series, and the maximum number of ligands exchange was found to be 3. No correlation was found between heteroatom and heteroligand substitution reactions, indicating independent mechanisms. The metal atom exchange mechanism likely involves ligands, but those ligands remained where they were at the beginning of the reaction, whether in the ligand complex or on the cluster. It was found that metal substitution reaction was more efficient than ligand substitution, but it is not clear if they were determined by thermodynamics or kinetics.

Second, experimental results for only ligand substitution onto  $\text{M}_4\text{Ag}_{44}(\text{SR})_{30}$  clusters were also presented, using different ligands. The study showed random substitution for both 4-HSC<sub>6</sub>H<sub>4</sub>OH and 4-FTP ligands, with numbers of substitutions well beyond 6, confirming no final site preference for ligands on  $\text{M}_4\text{Ag}_{44}(\text{p-MBA})_{30}$  clusters. It was found that the average number of substitutions for both ligands was close to but less than the input ratio. Also, both exchange reactions were found to be product-favored. Halogen substituted thiophenols were used to investigate the nature of the ligand substitution and the ligand substitution reactions on  $\text{M}_4\text{Ag}_{44}(\text{p-MBA})_{30}$  were found to be electrophilic in nature.

## References

1. Hornyak, G. L.; Tibbals, H. F.; Dutta, J.; Moore, J. J., *Introduction to nanoscience & nanotechnology*. CRC Press: Boca Raton; London; New York, 2009.
2. Ashby, M. F.; Ferreira, P. J.; Schodek, D. L., Chapter 2 - An Evolutionary Perspective. In *Nanomaterials, Nanotechnologies and Design*, Ashby, M. F.; Ferreira, P. J.; Schodek, D. L., Eds. Butterworth-Heinemann: Boston, 2009; pp 17-39.
3. Faraday, M., The Bakerian Lecture: Experimental Relations of Gold (and Other Metals) to Light. *Philosophical Transactions of the Royal Society of London* **1857**, *147*, 145-181.
4. Feynman, R. P., There's plenty of room at the bottom [data storage]. *Journal of Microelectromechanical Systems* **1992**, *1* (1), 60-66.
5. Mathew, A.; Pradeep, T., Noble Metal Clusters: Applications in Energy, Environment, and Biology. *Particle & Particle Systems Characterization* **2014**, *31* (10), 1017-1053.
6. Jin, R., Quantum sized, thiolate-protected gold nanoclusters. *Nanoscale* **2010**, *2* (3), 343-362.

7. Jin, R.; Zeng, C.; Zhou, M.; Chen, Y., Atomically Precise Colloidal Metal Nanoclusters and Nanoparticles: Fundamentals and Opportunities. *Chemical Reviews* **2016**, *116* (18), 10346-10413.
8. Chakraborty, I.; Pradeep, T., Atomically Precise Clusters of Noble Metals: Emerging Link between Atoms and Nanoparticles. *Chem Rev* **2017**, *117* (12), 8208-8271.
9. Chen, S.; Ingram, R. S.; Hostetler, M. J.; Pietron, J. J.; Murray, R. W.; Schaaff, T. G.; Khoury, J. T.; Alvarez, M. M.; Whetten, R. L., Gold nanoelectrodes of varied size: transition to molecule-like charging. *Science* **1998**, *280* (5372), 2098-101.
10. Dolamic, I.; Knoppe, S.; Dass, A.; Bürgi, T., First enantioseparation and circular dichroism spectra of Au<sub>38</sub> clusters protected by achiral ligands. *Nature Communications* **2012**, *3* (1), 798.
11. Desireddy, A.; Conn, B. E.; Guo, J.; Yoon, B.; Barnett, R. N.; Monahan, B. M.; Kirschbaum, K.; Griffith, W. P.; Whetten, R. L.; Landman, U.; Bigioni, T. P., Ultrastable silver nanoparticles. *Nature* **2013**, *501* (7467), 399-402.
12. Taglietti, A.; Diaz Fernandez, Y. A.; Amato, E.; Cucca, L.; Dacarro, G.; Grisoli, P.; Necchi, V.; Pallavicini, P.; Pasotti, L.; Patrini, M., Antibacterial activity of glutathione-coated silver nanoparticles against gram positive and gram negative bacteria. *Langmuir* **2012**, *28* (21), 8140-8148.
13. Le Ouay, B.; Stellacci, F., Antibacterial activity of silver nanoparticles: A surface science insight. *Nano Today* **2015**, *10* (3), 339-354.
14. Wang, K.; Wu, Y.; Li, H.; Li, M.; Zhang, D.; Feng, H.; Fan, H., Synthesis, characterization and antimicrobial activity of silver nanoparticles: Ag<sub>n</sub>(NALC)<sub>m</sub> and Ag<sub>n</sub>(GSHR)<sub>m</sub>. *RSC Advances* **2014**, *4* (10), 5130.

15. Zheng, K.; Yuan, X.; Goswami, N.; Zhang, Q.; Xie, J., Recent advances in the synthesis, characterization, and biomedical applications of ultrasmall thiolated silver nanoclusters. *RSC Advances* **2014**, *4* (105), 60581-60596.
16. Brust, M.; Walker, M.; Bethell, D.; Schiffrin, D. J.; Whyman, R., Synthesis of Thiol-derivatised Gold Nanoparticles in a Two-phase Liquid-Liquid System. *J. Chem. Soc., Chem. Commun.* **1994**, *1994* (7), 801-802.
17. Whetten, R. L.; Khoury, J. T.; Alvarez, M. M.; Murthy, S.; Vezmar, I.; Wang, Z. L.; Stephens, P. W.; Cleveland, C. L.; Luedtke, W. D.; Landman, U., Nanocrystal gold molecules. *Advanced Materials* **1996**, *8* (5), 428-433.
18. Terrill, R. H.; Postlethwaite, T. A.; Chen, C.-H.; Poon, C.-D.; Terzis, A.; Chen, A.; Hutchison, J. E.; Clark, M. R.; Wignall, G.; Londono, J. D.; Superfine, R.; Falvo, M.; Johnson, C. S. J.; Samulski, E. T.; Murray, R., Monolayers in three dimensions: NMR, SAXS, thermal, and electron hopping studies of alkanethiol stabilized gold clusters. *Journal of the American Chemical Society* **1995**, *117* (50), 12537-12548.
19. Hostetler, M. J.; Green, S. J.; Stokes, J. J.; Murray, R. W., Monolayers in Three Dimensions: Synthesis and Electrochemistry of  $\omega$ -Functionalized Alkanethiolate-Stabilized Gold Cluster Compounds. *Journal of the American Chemical Society* **1996**, *118* (17), 4212-4213.
20. Ingram, R. S.; Hostetler, M. J.; Murray, R. W.; Schaaff, T. G.; Khoury, J. T.; Whetten, R. L.; Bigioni, T. P.; Guthrie, D. K.; First, P. N., 28 kDa alkanethiolate-protected Au clusters give analogous solution electrochemistry and STM Coulomb staircases. *Journal of the American Chemical Society*. **1997**, *119* (39), 9279-9280.

21. Negishi, Y.; Takasugi, Y.; Sato, S.; Yao, H.; Kimura, K.; Tsukuda, T., Magic-Numbered Au<sub>n</sub> Clusters Protected by Glutathione Monolayers (n = 18, 21, 25, 28, 32, 39): Isolation and Spectroscopic Characterization. *Journal of the American Chemical Society* **2004**, *126* (21), 6518-6519.
22. Negishi, Y.; Nobusada, K.; Tsukuda, T., Glutathione-Protected Gold Clusters Revisited: Bridging the Gap between Gold(I)-Thiolate Complexes and Thiolate-Protected Gold Nanocrystals. *Journal of the American Chemical Society* **2005**, *127* (14), 5261-5270.
23. Jadzinsky, P. D.; Calero, G.; Ackerson, C. J.; Bushnell, D. A.; Kornberg, R. D., Structure of a thiol monolayer-protected gold nanoparticle at 1.1 Å resolution. *Science* **2007**, *318* (5849), 430-3.
24. Bakr, O. M.; Amendola, V.; Aikens, C. M.; Wenseleers, W.; Li, R.; Dal Negro, L.; Schatz, G. C.; Stellacci, F., Silver nanoparticles with broad multiband linear optical absorption. *Angewandte Chemie International Edition* **2009**, *48* (32), 5921-6.
25. Harkness, K. M.; Tang, Y.; Dass, A.; Pan, J.; Kothalawala, N.; Reddy, V. J.; Cliffel, D. E.; Demeler, B.; Stellacci, F.; Bakr, O. M.; McLean, J. A., Ag<sub>44</sub>(SR)<sub>30</sub><sup>4-</sup>: a silver-thiolate superatom complex. *Nanoscale* **2012**, *4* (14), 4269-74.
26. Kumar, S.; Bolan, M. D.; Bigioni, T. P., Glutathione-Stabilized Magic-Number Silver Cluster Compounds. *Journal of the American Chemical Society* **2010**, *132* (38), 13141-13143.
27. Knight, W. D.; Clemenger, K.; de Heer, W. A.; Saunders, W. A.; Chou, M. Y.; Cohen, M. L., Electronic Shell Structure and Abundances of Sodium Clusters. *Physical Review Letters* **1984**, *52* (24), 2141-2143.

28. de Heer, W. A., The physics of simple metal clusters: experimental aspects and simple models. *Reviews of Modern Physics* **1993**, 65 (3), 611-676.
29. Walter, M.; Akola, J.; Lopez-Acevedo, O.; Jadzinsky, P. D.; Calero, G.; Ackerson, C. J.; Whetten, R. L.; Grönbeck, H.; Häkkinen, H., A unified view of ligand-protected gold clusters as superatom complexes. *Proceedings of the National Academy of Sciences* **2008**, 105 (27), 9157-9162.
30. Nishigaki, J.; Koyasu, K.; Tsukuda, T., Chemically modified gold superatoms and superatomic molecules. *Chemical record (New York, N.Y.)* **2014**, 14 (5), 897-909.
30. Walter, M.; Akola, J.; Lopez-Acevedo, O.; Jadzinsky, P. D.; Calero, G.; Ackerson, C. J.; Whetten, R. L.; Grönbeck, H.; Häkkinen, H., A unified view of ligand-protected gold clusters as superatom complexes. *Proceedings of the National Academy of Sciences* **2008**, 105 (27), 9157.
32. Negishi, Y.; Chaki, N. K.; Shichibu, Y.; Whetten, R. L.; Tsukuda, T., Origin of Magic Stability of Thiolated Gold Clusters: A Case Study on Au<sub>25</sub>(SC<sub>6</sub>H<sub>13</sub>)<sub>18</sub>. *Journal of the American Chemical Society* **2007**, 129 (37), 11322-11323.
33. Xu, W. W.; Gao, Y., Unraveling the Atomic Structures of the Au<sub>68</sub>(SR)<sub>34</sub> Nanoparticles. *The Journal of Physical Chemistry C* **2015**, 119 (25), 14224-14229.
34. Jadzinsky, P. D.; Calero, G.; Ackerson, C. J.; Bushnell, D. A.; Kornberg, R. D., Structure of a Thiol Monolayer-Protected Gold Nanoparticle at 1.1 Å Resolution. *Science* **2007**, 318 (5849), 430-433.
35. Terrill, R. H.; Postlethwaite, T. A.; Chen, C.-h.; Poon, C.-D.; Terzis, A.; Chen, A.; Hutchison, J. E.; Clark, M. R.; Wignall, G., Monolayers in Three Dimensions: NMR, SAXS, Thermal, and Electron Hopping Studies of Alkanethiol Stabilized

- Gold Clusters. *Journal of the American Chemical Society* **1995**, *117* (50), 12537-12548.
36. Hostetler, M. J.; Stokes, J. J.; Murray, R. W., Infrared Spectroscopy of Three-Dimensional Self-Assembled Monolayers: N-Alkanethiolate Monolayers on Gold Cluster Compounds. *Langmuir* **1996**, *12* (15), 3604-3612.
37. Dass, A., Mass Spectrometric Identification of Au<sub>68</sub>(SR)<sub>34</sub> Molecular Gold Nanoclusters with 34-Electron Shell Closing. *Journal of the American Chemical Society* **2009**, *131* (33), 11666-11667.
38. Dharmaratne, A. C.; Krick, T.; Dass, A., Nanocluster Size Evolution Studied by Mass Spectrometry in Room Temperature Au<sub>25</sub>(SR)<sub>18</sub> Synthesis. *Journal of the American Chemical Society* **2009**, *131* (38), 13604-13605.
39. Luo, Z.; Nachammai, V.; Zhang, B.; Yan, N.; Leong, D. T.; Jiang, D.; Xie, J., Toward Understanding the Growth Mechanism: Tracing All Stable Intermediate Species from Reduction of Au(I)-Thiolate Complexes to Evolution of Au<sub>25</sub> Nanoclusters. *Journal of the American Chemical Society* **2014**, *136* (30), 10577-10580.
40. Schaaff, T. G.; Knight, G.; Shafiqullin, M. N.; Borkman, R. F.; Whetten, R. L., Isolation and Selected Properties of a 10.4 kDa Gold:Glutathione Cluster Compound. *The Journal of Physical Chemistry B* **1998**, *102* (52), 10643-10646.
41. Kroto, H. W.; Heath, J. R.; O'Brien, S. C.; Curl, R. F.; Smalley, R. E., C<sub>60</sub> Buckminsterfullerene. *Nature* **1985**, *318*, 162.
42. Gross, D. H. E.; Madjet, M. E., Fragmentation phase transition in atomic clusters IV. *Zeitschrift für Physik B Condensed Matter* **1997**, *104* (3), 541-551.

43. Morse, M. D., Clusters of transition-metal atoms. *Chemical Reviews* **1986**, *86* (6), 1049-1109.
44. Harkness, K. M.; Cliffel, D. E.; McLean, J. A., Characterization of thiolate-protected gold nanoparticles by mass spectrometry. *The Analyst* **2010**, *135* (5), 868-874.
45. Logunov, S. L.; Ahmadi, T. S.; El-Sayed, M. A.; Khoury, J. T.; Whetten, R. L., Electron Dynamics of Passivated Gold Nanocrystals Probed by Subpicosecond Transient Absorption Spectroscopy. *The Journal of Physical Chemistry B* **1997**, *101* (19), 3713-3719.
46. Jin, R.; Zeng, C.; Zhou, M.; Chen, Y., Atomically Precise Colloidal Metal Nanoclusters and Nanoparticles: Fundamentals and Opportunities. *Chemical Reviews* **2016**, *116*.(18), 10346–413.
47. Hicks, J. F.; Templeton, A. C.; Chen, S.; Sheran, K. M.; Jasti, R.; Murray, R. W.; Debord, J.; Schaaff, T. G.; Whetten, R. L., The monolayer thickness dependence of quantized double-layer capacitances of monolayer-protected gold clusters. *Anal Chem* **1999**, *71* (17), 3703-11.
48. Schaaff, T. G.; Whetten, R. L., Giant Gold–Glutathione Cluster Compounds: Intense Optical Activity in Metal-Based Transitions. *The Journal of Physical Chemistry B* **2000**, *104* (12), 2630-2641.
49. Ingram, R. S.; Hostetler, M. J.; Murray, R. W., Poly-hetero- $\omega$ -functionalized Alkanethiolate-Stabilized Gold Cluster Compounds. *Journal of the American Chemical Society* **1997**, *119* (39), 9175-9178.

50. Templeton, A. C.; Cliffel, D. E.; Murray, R. W., Redox and Fluorophore Functionalization of Water-Soluble, Tiopronin-Protected Gold Clusters. *Journal of the American Chemical Society* **1999**, *121* (30), 7081-7089.
51. Lu, Y.; Chen, W., Sub-nanometre sized metal clusters: from synthetic challenges to the unique property discoveries. *Chemical Society Reviews* **2012**, *41* (9), 3594-3623.
52. Sankar, M.; Dimitratos, N.; Miedziak, P. J.; Wells, P. P.; Kiely, C. J.; Hutchings, G. J., Designing bimetallic catalysts for a green and sustainable future. *Chemical Society Reviews* **2012**, *41* (24), 8099-8139.
53. Ferrando, R.; Jellinek, J.; Johnston, R. L., Nanoalloys: From Theory to Applications of Alloy Clusters and Nanoparticles. *Chemical Reviews* **2008**, *108* (3), 845-910.
54. Zhang, H.; Watanabe, T.; Okumura, M.; Haruta, M.; Toshima, N., Catalytically highly active top gold atom on palladium nanocluster. *Nature Materials* **2012**, *11* (1), 49-52..
55. Toshima, N.; Yonezawa, T., Bimetallic nanoparticles—novel materials for chemical and physical applications. *New Journal of Chemistry* **1998**, *22* (11), 1179-1201.
56. Wu, Z.; Jin, R., On the Ligand's Role in the Fluorescence of Gold Nanoclusters. *Nano Letters* **2010**, *10* (7), 2568-2573.
57. Shibu, E. S.; Muhammed, M. A. H.; Tsukuda, T.; Pradeep, T., Ligand Exchange of Au<sub>25</sub>SG<sub>18</sub> Leading to Functionalized Gold Clusters: Spectroscopy, Kinetics, and Luminescence. *The Journal of Physical Chemistry C* **2008**, *112* (32), 12168-12176.
58. Knoppe, S.; Bürgi, T., Chirality in Thiolate-Protected Gold Clusters. *Accounts of Chemical Research* **2014**, *47* (4), 1318-1326.

59. Zhu, M.; Qian, H.; Meng, X.; Jin, S.; Wu, Z.; Jin, R., Chiral Au<sub>25</sub> Nanospheres and Nanorods: Synthesis and Insight into the Origin of Chirality. *Nano Letters* **2011**, *11* (9), 3963-3969..
60. Negishi, Y.; Kamimura, U.; Ide, M.; Hirayama, M., A photoresponsive Au<sub>25</sub> nanocluster protected by azobenzene derivative thiolates. *Nanoscale* **2012**, *4* (14), 4263-4268.
61. Gilroy, K. D.; Ruditskiy, A.; Peng, H.-C.; Qin, D.; Xia, Y., Bimetallic Nanocrystals: Syntheses, Properties, and Applications. *Chemical Reviews* **2016**, *116* (18), 10414-10472.
62. Yuan, X.; Dou, X.; Zheng, K.; Xie, J., Recent Advances in the Synthesis and Applications of Ultrasmall Bimetallic Nanoclusters. *Particle & Particle Systems Characterization* **2015**, *32* (6), 613-629.
63. Choi, J.-P.; Fields-Zinna, C. A.; Stiles, R. L.; Balasubramanian, R.; Douglas, A. D.; Crowe, M. C.; Murray, R. W., Reactivity of [Au<sub>25</sub>(SCH<sub>2</sub>CH<sub>2</sub>Ph)<sub>18</sub>]<sup>1-</sup> Nanoparticles with Metal Ions. *The Journal of Physical Chemistry C* **2010**, *114* (38), 15890-15896.
64. Wu, Z., Anti-Galvanic Reduction of Thiolate-Protected Gold and Silver Nanoparticles. *Angewandte Chemie International Edition* **2012**, *51* (12), 2934-2938.
65. Jin, S.; Du, W.; Wang, S.; Kang, X.; Chen, M.; Hu, D.; Chen, S.; Zou, X.; Sun, G.; Zhu, M., Thiol-Induced Synthesis of Phosphine-Protected Gold Nanoclusters with Atomic Precision and Controlling the Structure by Ligand/Metal Engineering. *Inorganic Chemistry* **2017**, *56* (18), 11151-11159.
66. Li, Q.; Lambright, K. J.; Taylor, M. G.; Kirschbaum, K.; Luo, T.-Y.; Zhao, J.; Mpourmpakis, G.; Mokashi-Punekar, S.; Rosi, N. L.; Jin, R., Reconstructing the

- Surface of Gold Nanoclusters by Cadmium Doping. *Journal of the American Chemical Society* **2017**, *139* (49), 17779-17782.
67. Chen, Y.; Zeng, C.; Liu, C.; Kirschbaum, K.; Gayathri, C.; Gil, R. R.; Rosi, N. L.; Jin, R., *Journal of the American Chemical Society*. **2015**, *137*, 10076.
68. Kang, X.; Xiong, L.; Wang, S.; Yu, H.; Jin, S.; Song, Y.; Chen, T.; Zheng, L.; Pan, C.; Pei, Y.; Zhu, M., Shape-Controlled Synthesis of Trimetallic Nanoclusters: Structure Elucidation and Properties Investigation. *Chemistry – A European Journal* **2016**, *22* (48), 17145-17150..
69. Shon, Y.-S.; Dawson, G. B.; Porter, M.; Murray, R. W., Monolayer-Protected Bimetal Cluster Synthesis by Core Metal Galvanic Exchange Reaction. *Langmuir* **2002**, *18* (10), 3880-3885..
70. Krishnadas, K. R.; Baksi, A.; Ghosh, A.; Natarajan, G.; Pradeep, T., Structure-conserving spontaneous transformations between nanoparticles. *Nature Communications* **2016**, *7* (1), 13447.
71. Zhang, B.; Salassa, G.; Bürgi, T., Silver migration between Au<sub>38</sub>(SC<sub>2</sub>H<sub>4</sub>Ph)<sub>24</sub> and doped Ag<sub>x</sub>Au<sub>38-x</sub>(SC<sub>2</sub>H<sub>4</sub>Ph)<sub>24</sub> nanoclusters. *Chemical Communications* **2016**, *52* (59), 9205-9207.
72. Zhang, B.; Safonova, O. V.; Pollitt, S.; Salassa, G.; Sels, A.; Kazan, R.; Wang, Y.; Rupprechter, G.; Barrabés, N.; Bürgi, T., On the mechanism of rapid metal exchange between thiolate-protected gold and gold/silver clusters: a time-resolved in situ XAFS study. *Physical Chemistry Chemical Physics* **2018**, *20* (7), 5312-5318.
73. Bootharaju, M. S.; Sinatra, L.; Bakr, O. M., Distinct metal-exchange pathways of doped Ag<sub>25</sub> nanoclusters. *Nanoscale* **2016**, *8* (39), 17333-17339.

74. Wu, Z., *Angewandte Chemie International Edition*. **2012**, *51*, 2934..
75. Wang, M.; Wu, Z.; Chu, Z.; Yang, J.; Yao, C., Chemico-physical synthesis of surfactant- and ligand-free gold nanoparticles and their anti-galvanic reduction property. *Chem Asian J* **2014**, *9* (4), 1006-1010.
76. Negishi, Y.; Munakata, K.; Ohgake, W.; Nobusada, K., Effect of Copper Doping on Electronic Structure, Geometric Structure, and Stability of Thiolate-Protected Au<sub>25</sub> Nanoclusters. *The Journal of Physical Chemistry Letters* **2012**, *3* (16), 2209-2214..
77. Conn, B. E.; Atnagulov, A.; Bhattarai, B.; Yoon, B.; Landman, U.; Bigioni, T. P., Synthetic and Postsynthetic Chemistry of M<sub>4</sub>Au<sub>x</sub>Ag<sub>44-x</sub>(p-MBA)<sub>30</sub> Alloy
78. Wang, S.; Song, Y.; Jin, S.; Liu, X.; Zhang, J.; Pei, Y.; Meng, X.; Chen, M.; Li, P.; Zhu, M., Metal Exchange Method Using Au<sub>25</sub> Nanoclusters as Templates for Alloy Nanoclusters with Atomic Precision. *Journal of the American Chemical Society* **2015**, *137* (12), 4018-4021.
79. Yao, C.; Lin, Y.-j.; Yuan, J.; Liao, L.; Zhu, M.; Weng, L.-h.; Yang, J.; Wu, Z., Mono-cadmium vs Mono-mercury Doping of Au<sub>25</sub> Nanoclusters. *Journal of the American Chemical Society* **2015**, *137* (49), 15350-15353.
80. Liao, L.; Zhou, S.; Dai, Y.; Liu, L.; Yao, C.; Fu, C.; Yang, J.; Wu, Z., Mono-Mercury Doping of Au<sub>25</sub> and the HOMO/LUMO Energies Evaluation Employing Differential Pulse Voltammetry. *Journal of the American Chemical Society* **2015**, *137* (30), 9511-9514.
81. Yang, S.; Wang, S.; Jin, S.; Chen, S.; Sheng, H.; Zhu, M., A metal exchange method for thiolate-protected tri-metal M<sub>1</sub>Ag<sub>x</sub>Au<sub>24-x</sub>(SR)<sub>180</sub> (M = Cd/Hg) nanoclusters. *Nanoscale* **2015**, *7* (22), 10005-10007.

82. Bootharaju, M. S.; Joshi, C. P.; Parida, M. R.; Mohammed, O. F.; Bakr, O. M., Templated Atom-Precise Galvanic Synthesis and Structure Elucidation of a  $[\text{Ag}_{24}\text{Au}(\text{SR})_{18}]$  Nanocluster. *Angewandte Chemie International Edition* **2016**, *55* (3), 922-6.
83. Bootharaju, M. S.; Sinatra, L.; Bakr, O. M., Distinct metal-exchange pathways of doped  $\text{Ag}_{25}$  nanoclusters. *Nanoscale* **2016**, *8* (39), 17333-17339.
84. Zhang, B.; Bürgi, T., Doping Silver Increases the  $\text{Au}_{38}(\text{SR})_{24}$  Cluster Surface Flexibility. *The Journal of Physical Chemistry C* **2016**, *120* (8), 4660-4666.
85. Peng, X.; Manna, L.; Yang, W.; Wickham, J.; Scher, E.; Kadavanich, A.; Alivisatos, A. P., Shape control of CdSe nanocrystals. *Nature* **2000**, *404* (6773), 59-61.
86. Burrows, N. D.; Vartanian, A. M.; Abadeer, N. S.; Grzincic, E. M.; Jacob, L. M.; Lin, W.; Li, J.; Dennison, J. M.; Hinman, J. G.; Murphy, C. J., Anisotropic Nanoparticles and Anisotropic Surface Chemistry. *The Journal of Physical Chemistry Letters* **2016**, *7* (4), 632-41.
87. Hostetler, M. J.; Templeton, A. C.; Murray, R. W., Dynamics of Place-Exchange Reactions on Monolayer-Protected Gold Cluster Molecules. *Langmuir* **1999**, *15* (11), 3782-3789.
88. Song, Y.; Murray, R. W., Dynamics and Extent of Ligand Exchange Depend on Electronic Charge of Metal Nanoparticles. *Journal of the American Chemical Society* **2002**, *124* (24), 7096-7102.
89. Underwood, S.; Mulvaney, P., Effect of the Solution Refractive Index on the Color of Gold Colloids. *Langmuir* **1994**, *10* (10), 3427-3430.

90. Chen, S.; Templeton, A. C.; Murray, R. W., Monolayer-Protected Cluster Growth Dynamics. *Langmuir* **2000**, *16* (7), 3543-3548.
91. Mirkin, C. A.; Letsinger, R. L.; Mucic, R. C.; Storhoff, J. J., A DNA-based method for rationally assembling nanoparticles into macroscopic materials. *Nature* **1996**, *382* (6592), 607-9.
92. Kim, Y.; Johnson, R. C.; Hupp, J. T., Gold Nanoparticle-Based Sensing of “Spectroscopically Silent” Heavy Metal Ions. *Nano Letters* **2001**, *1* (4), 165-167.
93. Shichibu, Y.; Negishi, Y.; Tsukuda, T.; Teranishi, T., Large-Scale Synthesis of Thiolated Au<sub>25</sub> Clusters via Ligand Exchange Reactions of Phosphine-Stabilized Au<sub>11</sub> Clusters. *Journal of the American Chemical Society* **2005**, *127* (39), 13464-13465.
94. Dass, A.; Theivendran, S.; Nimmala, P. R.; Kumara, C.; Jupally, V. R.; Fortunelli, A.; Sementa, L.; Barcaro, G.; Zuo, X.; Noll, B. C., Au<sub>133</sub>(SPh-tBu)<sub>52</sub> nanomolecules: X-ray crystallography, optical, electrochemical, and theoretical analysis. *Journal of the American Chemical Society* **2015**, *137* (14), 4610-4613.
95. Guo, R.; Song, Y.; Wang, G.; Murray, R. W., Does Core Size Matter in the Kinetics of Ligand Exchanges of Monolayer-Protected Au Clusters? *Journal of the American Chemical Society* **2005**, *127* (8), 2752-2757.
96. Tracy, J. B.; Crowe, M. C.; Parker, J. F.; Hampe, O.; Fields-Zinna, C. A.; Dass, A.; Murray, R. W., Electrospray Ionization Mass Spectrometry of Uniform and Mixed Monolayer Nanoparticles: Au<sub>25</sub>[S(CH<sub>2</sub>)<sub>2</sub>Ph]<sub>18</sub> and Au<sub>25</sub>[S(CH<sub>2</sub>)<sub>2</sub>Ph]<sub>18-x</sub>(SR)<sub>x</sub>. *Journal of the American Chemical Society* **2007**, *129* (51), 16209-16215.

97. Ni, T. W.; Tofanelli, M. A.; Phillips, B. D.; Ackerson, C. J., Structural Basis for Ligand Exchange on Au<sub>25</sub>(SR)<sub>18</sub>. *Inorganic Chemistry* **2014**, *53* (13), 6500-6502.
98. Heinecke, C. L.; Ni, T. W.; Malola, S.; Mäkinen, V.; Wong, O. A.; Häkkinen, H.; Ackerson, C. J., Structural and theoretical basis for ligand exchange on thiolate monolayer protected gold nanoclusters. *Journal of the American Chemical Society* **2012**, *134* (32), 13316-22.
99. Fernando, A.; Aikens, C. M., Ligand Exchange Mechanism on Thiolate Monolayer Protected Au<sub>25</sub>(SR)<sub>18</sub> Nanoclusters. *The Journal of Physical Chemistry C* **2015**, *119* (34), 20179-20187.
100. Akola, J.; Kacprzak, K. A.; Lopez-Acevedo, O.; Walter, M.; Grönbeck, H.; Häkkinen, H., Thiolate-Protected Au<sub>25</sub> Superatoms as Building Blocks: Dimers and Crystals. *The Journal of Physical Chemistry C* **2010**, *114* (38), 15986-15994.
101. Niihori, Y.; Uchida, C.; Kurashige, W.; Negishi, Y., High-resolution separation of thiolate-protected gold clusters by reversed-phase high-performance liquid chromatography. *Physical Chemistry Chemical Physics* **2016**, *18* (6), 4251-4265.
102. Bootharaju, M. S.; Burlakov, V. M.; Besong, T. M. D.; Joshi, C. P.; AbdulHalim, L. G.; Black, D. M.; Whetten, R. L.; Goriely, A.; Bakr, O. M., Reversible Size Control of Silver Nanoclusters via Ligand-Exchange. *Chemistry of Materials* **2015**, *27* (12), 4289-4297.